Received: 22 October 2021 | Revised: 31 March 2022 | Accepted: 5 April 2022

DOI: 10.1111/mmi.14904

RESEARCH ARTICLE

WILEY

The *Plasmodium falciparum* parasitophorous vacuole protein P113 interacts with the parasite protein export machinery and maintains normal vacuole architecture

Hayley E. Bullen[1,2] | Paul R. Sanders[1] | Madeline G. Dans[1,3,4] | Thorey K. Jonsdottir[1,2] | David T. Riglar[4,5] | Oliver Looker[1] | Catherine S. Palmer[1] | Betty Kouskousis[1] | Sarah C. Charnaud[1] | Tony Triglia[4,5] | Mikha Gabriela[1,3,4] | Molly Parkyn Schneider[1] | Jo-Anne Chan[1,6] | Tania F. de Koning-Ward[3] | Jake Baum[4,5] | James W. Kazura[7] | James G. Beeson[1,6,8] | Alan F. Cowman[4,5] | Paul R. Gilson[1,2] | Brendan S. Crabb[1,2]

[1]Burnet Institute, Melbourne, Victoria, Australia

[2]Department of Microbiology and Immunology, University of Melbourne, Parkville, Victoria, Australia

[3]School of Medicine, Deakin University, Geelong, Victoria, Australia

[4]Walter and Eliza Hall Institute, Parkville, Victoria, Australia

[5]Department of Medical Biology, University of Melbourne, Parkville, Victoria, Australia

[6]Department of Medicine, University of Melbourne, Parkville, Victoria, Australia

[7]Centre for Global Health and Diseases, Case Western Reserve University, Cleveland, Ohio, USA

[8]Department of Immunology, Central Clinical School, Monash University, Melbourne, Victoria, Australia

Correspondence
Hayley E. Bullen, Burnet Institute, Life Sciences, 85 Commercial Road, Prahran, Melbourne, VIC 3004, Australia.
Email: hayley.bullen@burnet.edu.au

Present address
David T. Riglar, Imperial College London, Department of Infectious Diseases, South Kensington, London, UK

Catherine S. Palmer, Bio21, Parkville, Victoria, Australia

Sarah C. Charnaud, WHO, Geneva, Switzerland

Jake Baum, School of Medical Sciences, UNSW Kensington Campus, New South Wales, Australia

Thorey K. Jonsdottir, Department of Molecular Biology, Umeå University, Umeå, Sweden

Brendan S. Crabb, Department of Immunology and Pathology, Monash University, Melbourne, Australia

Tania F. de Koning-Ward, The Institute for Mental and Physical Health and Clinical Translation, Deakin University, Geelong, Victoria, Australia

Funding information
National Health and Medical Research Council, Grant/Award Number: APP1128198

Abstract

Infection with *Plasmodium falciparum* parasites results in approximately 627,000 deaths from malaria annually. Key to the parasite's success is their ability to invade and subsequently grow within human erythrocytes. Parasite proteins involved in parasite invasion and proliferation are therefore intrinsically of great interest, as targeting

Paul R. Gilson and Brendan S. Crabb contributed equally to this work.

these proteins could provide novel means of therapeutic intervention. One such protein is P113 which has been reported to be both an invasion protein and an intracellular protein located within the parasitophorous vacuole (PV). The PV is delimited by a membrane (PVM) across which a plethora of parasite-specific proteins are exported via the *Plasmodium* Translocon of Exported proteins (PTEX) into the erythrocyte to enact various immune evasion functions. To better understand the role of P113 we isolated its binding partners from in vitro cultures of *P. falciparum*. We detected interactions with the protein export machinery (PTEX and exported protein-interacting complex) and a variety of proteins that either transit through the PV or reside on the parasite plasma membrane. Genetic knockdown or partial deletion of P113 did not significantly reduce parasite growth or protein export but did disrupt the morphology of the PVM, suggesting that P113 may play a role in maintaining normal PVM architecture.

KEYWORDS
blebs, erythrocyte, invasion, *Plasmodium falciparum*, protein trafficking, vacuole

1 | INTRODUCTION

Plasmodium spp. of the phylum Apicomplexa are the major causative agents of malaria disease in humans. In 2019 they were responsible for approximately 627,000 deaths (WHO, 2021), with the majority of infections occurring in women and children under 5 years old, and over 90% due to infection with *Plasmodium falciparum*. Key factors such as increasing drug resistance to current first-line antimalarials have compelled the continued study of the parasite's biology. Parasite-derived proteins which function at multiple life stages are a priority for functional investigation as they potentially represent novel drug targets. Here, we have investigated the function of P113 (PF3D7_1420700); a merozoite surface (Galaway et al., 2017) and parasitophorous vacuole (PV)-resident protein (Batinovic et al., 2017; Elsworth et al., 2016) identified as interacting with the invasion-associated ligand Rh5 (Campeotto et al., 2020; Galaway et al., 2017), the *Plasmodium* Translocon of Exported proteins (PTEX) (Elsworth et al., 2016), and PTEX cargo proteins of the SURFIN family (Miyazaki et al., 2021).

PTEX, the machinery responsible for exporting proteins across the PV membrane (PVM) and into the erythrocyte cytosol (Beck et al., 2014; de Koning-Ward et al., 2009; Elsworth et al., 2014; Ho et al., 2018) is essential for parasite survival (Beck et al., 2014; Elsworth et al., 2014). This parasite-derived machine serves to transport parasite proteins into the erythrocyte, whereupon they perform essential functions such as immune evasion, nutrient uptake, and likely waste disposal (Counihan et al., 2021; de Koning-Ward et al., 2016; Jonsdottir, Gabriela, et al., 2021). PTEX was originally identified in 2009 (de Koning-Ward et al., 2009) and is composed of three essential core proteins (EXP2, HSP101, and PTEX150) (Beck et al., 2014; Charnaud, Kumarasingha, et al., 2018; de Koning-Ward et al., 2009; Elsworth et al., 2014; Garten et al., 2018), and two non-essential auxiliary proteins (TRX2 and PTEX88) (Chisholm et al., 2016; de Koning-Ward et al., 2009; Matthews et al., 2013; Matz et al., 2013). Within this complex, the N-termini of seven EXP2 subunits form a pore through the PVM (Garten et al., 2018; Hakamada et al., 2017; Ho et al., 2018; Sanders et al., 2019). The remainder of EXP2 projects into the PV space where it binds seven subunits of the structural protein PTEX150, which together bind six subunits of the AAA+ ATPase HSP101 (Bullen et al., 2012; Ho et al., 2018). HSP101 unfolds proteins prior to extruding them through the remainder of PTEX for translocation into the erythrocyte compartment (Ho et al., 2018; Matthews et al., 2019). Protein unfolding is required for export through PTEX and exported protein cargoes fused with a conditionally unfoldable domain have been utilised as a tool to trap these proteins at the PVM to study PTEX functioning (Charnaud, Jonsdottir, et al., 2018; Gehde et al., 2009; Mesen-Ramirez et al., 2016).

Recently an additional complex residing within the PV space has been found to interact with PTEX: the exported protein-interacting complex (EPIC) (Batinovic et al., 2017; Hakamada et al., 2020; Morita et al., 2018). EPIC consists of three proteins, PV1/PV2/EXP3, and has been linked to PfEMP1 trafficking across the PVM via an auxiliary interaction with PTEX (Batinovic et al., 2017). Both EPIC and PTEX have been shown to interact with P113 via immunoprecipitation studies in *P. falciparum* (Batinovic et al., 2017; Elsworth et al., 2016) suggesting that P113 may also play an accessory role in PTEX functioning at the PVM. P113 was originally identified in the detergent resistant membrane (DRM) proteome of ring stage *P. falciparum* parasites and was predicted to interact with PTEX through its co-migration in the same Blue Native PAGE complexes as the essential PTEX component EXP2 (Sanders et al., 2005, 2007). This link was strengthened by data demonstrating

that P113 co-immunoprecipitates with the PTEX complex (Elsworth et al., 2016). Furthermore, recent work has implicated P113 in binding SURFIN4.1 mini proteins at the PVM prior to their export via PTEX to the infected erythrocyte surface (Miyazaki et al., 2021).

P113 was also detected in DRM fractions of schizont stage parasites and the predicted presence of a glycosylphosphatidylinositol (GPI) membrane anchor at the protein's C-terminus suggested it may also act during merozoite invasion of erythrocytes (Sanders et al., 2005). A recent study that made use of recombinantly expressed protein proposed that P113 may reside on the surface of the extracellular parasite and serve to pass an essential merozoite invasion protein, Rh5, to the CyRPA-RIPR complex to facilitate successful parasite invasion of erythrocytes (Campeotto et al., 2020; Galaway et al., 2017). Rh5/RIPR/CyRPA are parasite-specific proteins secreted from the apical secretory organelles of merozoites, where they interact with the erythrocyte surface protein basigin to facilitate merozoite invasion (Volz et al., 2016; Wong et al., 2019).

P113 orthologues are found in all *Plasmodium* species sequenced thus far, suggestive of a common and conserved function(s). Despite this, in the rodent model of malaria, *P. berghei*, *p113* knockout parasites are viable indicating the protein is not essential for asexual blood stage growth and invasion (Offeddu et al., 2014). The knockout parasites do, however, display defects in natural sporozoite transmission, leading to delayed patency in infected mice (Offeddu et al., 2014).

Given the important role of PTEX in protein export, understanding its molecular interactions will serve to strengthen our understanding of parasite biology and virulence. Here we sought to resolve the role of P113 throughout the asexual blood stage of *P. falciparum* parasites. We show that P113 localises to internal structures within the invading merozoite and following erythrocyte invasion, resides within the PV until late in the asexual cycle. Throughout the intraerythrocytic lifecycle, P113 is present within the PV space where it is likely bound to the PPM and extends across the PV space to interact with both PTEX and EPIC, as well as proteins destined for export into the erythrocyte. Removal of the C-terminal region of P113 causes it to become soluble, however, this has no effect on parasite growth, protein export or parasite invasion. Similarly, knockdown of P113 has no significant effect on parasite growth. However, reducing P113 expression by ~60–80%, or truncating the C-terminal region, results in the formation of large membranous blebs at the PVM. Overall, these data indicate that P113 plays a non-essential role in binding proteins within the PV space, and that this role is important for maintaining normal PV morphology.

2 | RESULTS

2.1 | P113 is expressed throughout the erythrocytic lifecycle and resides within the parasitophorous vacuole

P113 has a predicted molecular weight of ~112 kDa and its amino acid sequence comprises an N-terminal signal peptide, cysteine-rich region, central and C-terminal alpha-helical regions and a putative C-terminal GPI-anchor attachment signal sequence (Figure 1a). The N-terminal cysteine-rich region shows similarity to a rhamnose-binding lectin, however, it lacks the residues required for lectin binding (Campeotto et al., 2020). This region could therefore be involved in mediating protein–protein interactions. The alpha-helical regions are predicted to form coiled-coil regions and may aid in the formation of putative P113 homo-oligomers (Combet et al., 2000). Peptide antibodies (R1220 and R716) made in a previous study (Elsworth et al., 2016) to the N-terminal cysteine-rich region (Figure 1a) are used throughout this study.

To investigate the timing of P113 expression, ring, trophozoite, and schizont stage 3D7 parasites were harvested and analysed by western blot (Figure 1b). P113 migrated at 150 kDa as previously described (Elsworth et al., 2016) and is expressed throughout the intraerythrocytic lifecycle, reminiscent of PTEX components EXP2 and HSP101 (Figure 1b). P113 is predicted to be GPI anchored (Sanders et al., 2007) and this is consistent with its presence in the carbonate insoluble fraction upon carbonate extraction across the intraerythrocytic lifecycle (Figure 1c). Known PVM-associated protein EXP2 (Bullen et al., 2012; Ho et al., 2018) was used as a control for membrane-associated proteins, and HSP70-1 was used as a control for soluble proteins (Figure 1c, bottom two panels).

To investigate the compartmentalisation of P113 within the infected erythrocyte, we completed protease protection assays whereby trophozoite stage parasites were treated with either: equinatoxin (EQT, to lyse the erythrocyte membrane), equinatoxin and saponin (EQT + Sap, to lyse the erythrocyte and PVM) or equinatoxin, saponin and TX100 (EQT + Sap + TX100, to lyse all host and parasite membranes) in the presence or absence of increasing concentrations of proteinase K (PK) to digest the exposed proteins (Figure 1d). Consistent with our carbonate extraction data, protease protection assays demonstrated that P113 is strongly membrane associated and remains in the pellet fraction unless detergent (TX100) is used. Furthermore, P113 was protected from degradation when EQT alone was used, indicating that P113 is not present in the erythrocyte. In the presence of EQT and saponin, however, P113 was completely degraded upon addition of PK, indicating that P113 resides within the PV space (Figure 1d). These samples were also probed for the known PVM protein EXP2, which showed the same degradation pattern as P113, confirming that the solubilisation of the compartments had been effective (Figure S1) (Sanders et al., 2019). Human HSP70 was used as an erythrocyte protein control and was degraded by PK upon EQT treatment as previously reported (Figure S1) (Sanders et al., 2019).

2.2 | P113 is present in the PV throughout the intraerythrocytic cycle

To examine the localisation of P113 in intracellular parasites we created a P113 parasite line expressing a C-terminal haemagglutinin (HA) epitope tag (P113HA, Figures 2a, S2, Table S1), enabling us to localise P113 with a highly specific HA monoclonal antibody (Figure 2).

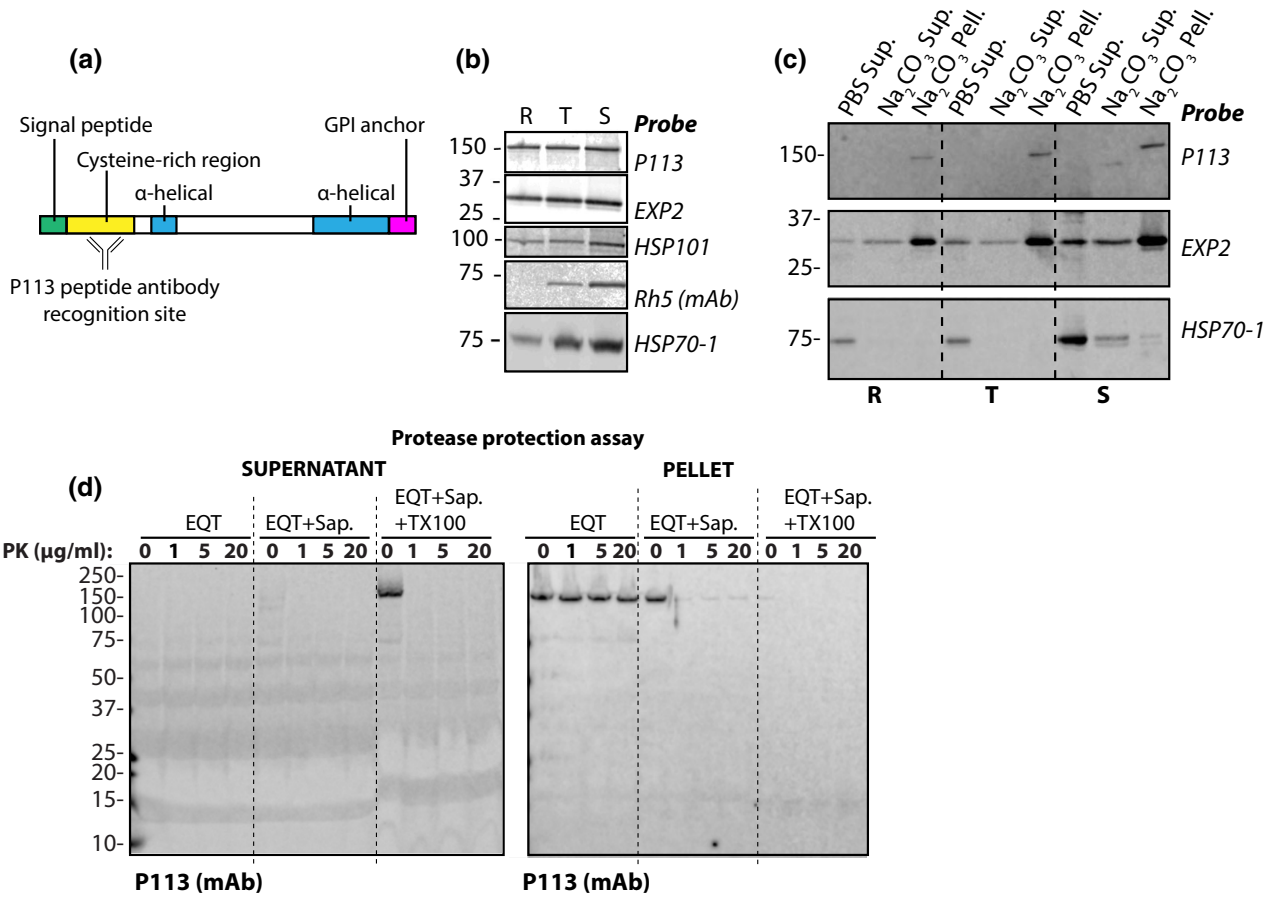

FIGURE 1 P113 is expressed throughout the intraerythrocytic lifecycle and is present within the parasitophorous vacuole space. (a) Schematic of P113 protein structure. (b) Parasite samples were collected at ring (R), trophozoite (T) and schizont (S) stage and probed with protein specific antibodies. P113 is expressed in all stages, as are PTEX proteins (EXP2 and HSP101), while the invasion-associated protein Rh5 is only expressed in later stages. HSP70-1 is constitutively expressed. Blots are representative of three independent biological replicates. R1220 was used to detect P113 (Elsworth et al., 2016). (c) Parasite samples were collected at ring (R), trophozoite (T) and schizont (S) stage and analysed by carbonate extraction assay. P113 is found within the carbonate insoluble fraction, along with the membrane protein EXP2. HSP70-1 is associated with the PBS soluble fraction as expected. Sup: Supernatant. Pell: Insoluble pellet fraction. Blots are representative of three independent biological replicates. R1220 was used to detect P113 (Elsworth et al., 2016). (d) Protease protection assays probed with the P113 mAb (Elsworth et al., 2016). Equinatoxin (EQT) permeabilises erythrocytes and allows proteinase K (PK) access to the erythrocyte contents. EQT + saponin (sap) permeabilises the erythrocyte and the PVM. EQT + sap+TX100 solubilises the erythrocyte, PVM and PPM. P113 is not digested by PK in the presence of EQT alone but is completely degraded by PK upon addition of saponin, indicating it resides within the PV space. Controls are displayed in Figure S1 and published in (Sanders et al., 2019). R1220 was used to detect P113 (Elsworth et al., 2016)

FIGURE 2 P113 colocalises with PTEX components throughout the intraerythrocytic cycle. (a) Cloning strategy used to generate P113HA line. The C-terminal third of the gene is flanked by LoxP sites and an HA-epitope tag is inserted upstream of the P113 GPI-anchor attachment site. (b) Western blot showing the specificity of the HA and P113 (R1220) (Elsworth et al., 2016) antibodies for detecting P113. PV1HA was used as a positive control for the HA antibody and 3D7 as a negative control. Bands of the correct size were detected for P113HA and PV1HA. * indicates non-specific bands. (c) Immediately post-invasion in ring stages (i) P113 colocalises with PTEX component EXP2 at the PV and maintains this localisation throughout the intraerythrocytic lifecycle in trophozoites (ii) through to early schizonts (iii). In mid-schizonts (iv) the PPM but not the PVM begins to invaginate around the developing merozoites. P113 can be detected around the nascent merozoites demonstrating P113 localises to the PPM face of PV space. In late stage schizonts (v/vi), P113 is no longer clearly present at the PPM as indicated by only partial co-labelling with the PPM marker $MSP1_{19}$. Instead P113 (possibly newly synthesised) appears to reside within internal structures, likely nascent secretory organelles. Scale bars: 5 µm. White arrow: PVM bleb. (d–i) immunofluorescence assays of merozoites co-labelled with HA (P113HA) and the PPM marker $MSP1_{19}$ (d), the dense granule markers PTEX150 (e) and EXP2 (f), the rhoptry markers Rh5 (g) and RhopH2 (h) and the microneme marker AMA1 (i). Pearson's correlation coefficients (r value) were calculated for at least 50 cells per antibody and data indicate that P113 most closely localises with the dense granules and rhoptries, and not the parasite surface and micronemes. Mean r and standard deviation (SD) are shown for each antibody. Scale bars: 1 µm. (j) IFA of invading merozoites analysed by widefield microscopy. RON4 labels the tight junction which forms between the erythrocyte and parasite during invasion. P113 is carried into the erythrocyte in internal structures in a manner like that seen for dense-granule-associated PTEX components (Riglar et al., 2013). Scale bars: 1 µm

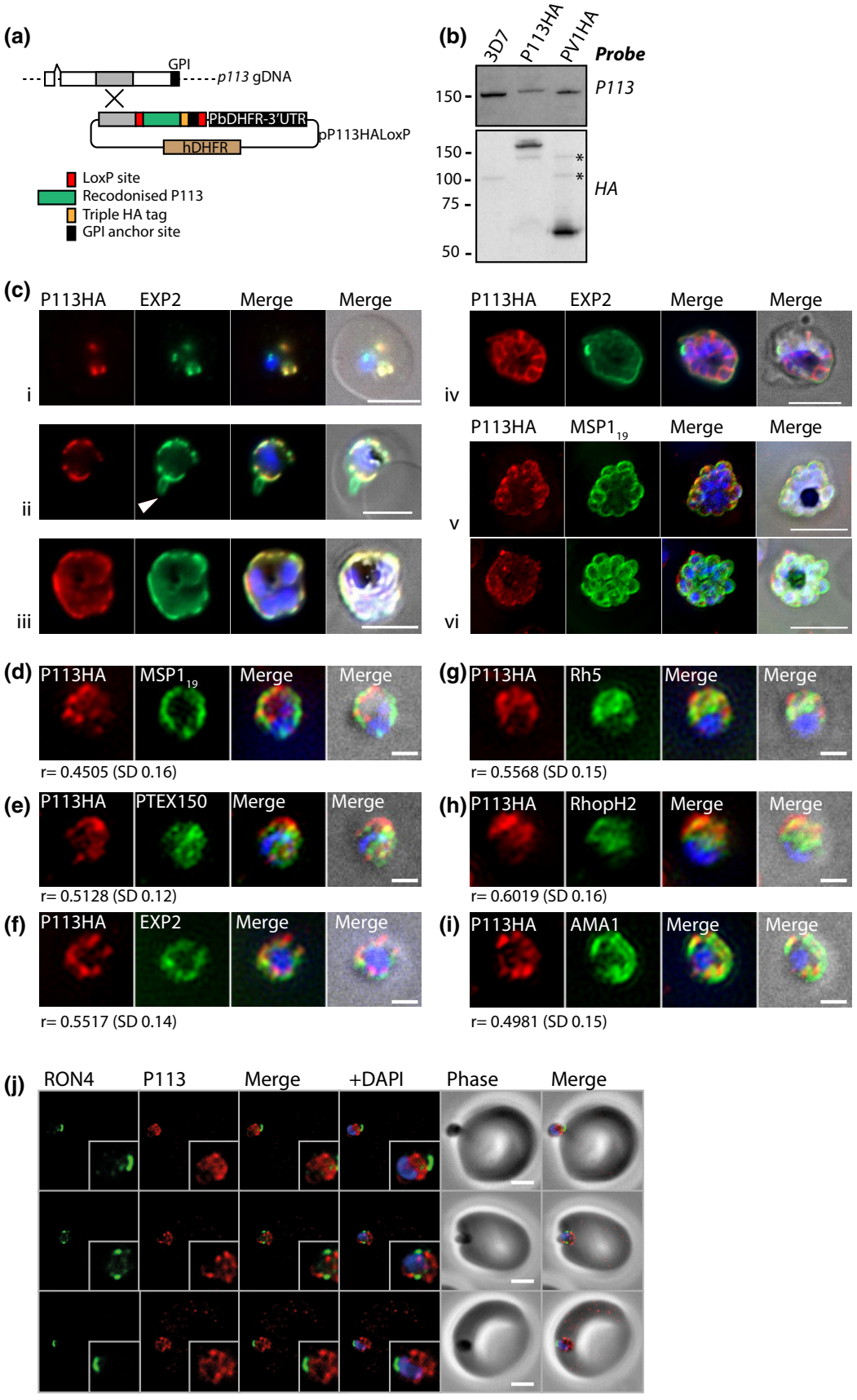
(a)
GPI
p113 gDNA
PbDHFR-3'UTR
hDHFR
pP113HALoxP
LoxP site
Recodonised P113
Triple HA tag
GPI anchor site
(b)
3D7
P113HA
PV1HA
Probe
P113
HA
150
100
75
50
(c)
P113HA
EXP2
Merge
i
ii
iii
iv
MSP1 19
v
vi
(d)
r= 0.4505 (SD 0.16)
(e)
PTEX150
r= 0.5128 (SD 0.12)
(f)
r= 0.5517 (SD 0.14)
(g)
Rh5
r= 0.5568 (SD 0.15)
(h)
RhopH2
r= 0.6019 (SD 0.16)
(i)
AMA1
r= 0.4981 (SD 0.15)
(j)
RON4
P113
+DAPI
Phase

The HA sequence was inserted upstream of the putative GPI-anchor attachment site to enable detection of the protein following cleavage of the putative GPI-anchor signal sequence (Figures 2a, S2a, Table S1). Western blotting analysis revealed that the P113HA band was, as expected, slightly larger than the endogenous protein when probed with the N-terminal P113 antibody (Figure 2b, top panel). The same band was also detected with a commercial anti-HA antibody indicating that the protein was correctly tagged (Figure 2b). PV1HA (Batinovic et al., 2017) was used as a positive control for the HA antibody and migrated as expected (Figure 2b). Co-labelling immunofluorescence assays (IFAs) were also completed in the P113HA line with the HA and P113 antibody (R716), and resultant data revealed that both antibodies label the same regions of the parasite (Figure S2b), and therefore the specific HA monoclonal antibody is suitable for further microscopic analysis of P113 localisation.

To determine the localisation of P113 during the intraerythrocytic lifecycle, IFAs were completed with the P113HA parasite line. These data revealed that immediately post-invasion when the parasite is amoeboid, P113 is present as discrete puncta that colocalise with PV-resident PTEX component EXP2 (Figure 2c,i). P113 labelling was also detected in the PV alongside EXP2 in trophozoites and early schizonts (Figure 2c,ii/iii) but is absent from EXP2-associated PVM blebs (Figure 2c,ii, white arrow). The PV is bordered by both the PPM and the PVM, therefore, to seek clarity on which membrane P113 was localised to, we examined mid-stage schizonts. During this stage, the PPM and the PVM begin to separate as individual daughter cells form. P113 can be seen invaginating around the nascent daughter cells, consistent with it being tethered to the PPM during the intraerythrocytic stage (Figure 2c,iv). During late stage schizogony (Figure 2c,v/vi), however, this surface expression appears to be gradually lost and P113 no longer colocalises with PPM marker $MSP1_{19}$ (Figure 2c,vi) and instead is present as diffuse puncta dispersed throughout the nascent merozoites. These data suggest that P113 is lost from the surface at a late stage of schizogony and newly formed P113 is present within nascent merozoites. These data are consistent with previous findings demonstrating that P113 is present in the PV until late schizogony (Miyazaki et al., 2021; Yam et al., 2013).

Previous data have suggested that P113 is present on the surface of merozoites (Galaway et al., 2017), however, our IFA analyses of late stage schizonts suggested that P113 is likely no longer present at the PPM at this stage. We therefore looked more closely at the localisation of P113 in merozoites (Figure 2d–j). Merozoites were co-labelled with anti-HA to detect P113HA, and either the PPM marker $MSP1_{19}$ (Figure 2d), the dense granule markers EXP2 and PTEX150 (Figure 2e,f), the rhoptry markers Rh5 and RhopH2 (Figure 2g,h) or the microneme marker AMA1 (Figure 2i). At least 50 cells were examined per antibody, and Pearson's correlation coefficients were produced (mean r values, Figure 2d–i), where r = 1 indicates complete colocalisation and r = 0 indicates no colocalisation. Data generated indicate that P113 shows the least colocalisation with $MSP1_{19}$ and therefore does not appear to be on the surface of the merozoites. Instead, P113 colocalised most strongly with dense granule (Figure 2e,f) and rhoptry (Figure 2h,i) markers, indicating that it is likely stored inside internal secretory organelles prior to its release into the nascent PV upon invasion (Figure 2c,i). This is consistent with previous data demonstrating that P113 colocalises with dense granule marker RESA in schizonts (Miyazaki et al., 2021).

During parasite invasion, some proteins are released from the secretory organelles (dense granules, rhoptries and micronemes) onto the merozoite surface to facilitate parasite invasion. These proteins are sequentially shed from the parasite plasma membrane as the parasite enters the erythrocyte by moving through a tight-junction formed between the merozoite and the point of contact with the erythrocyte (Weiss et al., 2015). Therefore, if P113 is released from internal secretory organelles and onto the surface of the erythrocyte during invasion, it would be expected to be shed from the parasite surface. If this is the case, P113 should not be visible in the internalised merozoite when probed specifically using the antibody generated to its N-terminus. Conversely, if it is maintained within the secretory organelles during invasion, it should be visible within the parasite upon completion of invasion. To investigate the localisation of P113 during invasion, invading merozoites were imaged by co-labelling with an antibody to the N-terminus of endogenous P113, and a marker of the tight junction, RON4 (Richard et al., 2010) (Figure 2j). RON4 sits at the interface between the internalised merozoite and the erythrocyte membrane. These images demonstrate that when the merozoite first contacts the erythrocyte and a tight junction is formed (Figure 2j, top panel), P113 labelling is behind that of RON4 and appears to be within internal structures. As the merozoite invades (Figure 2j, middle panel) this labelling remains inside the merozoite and moves past the tight junction. As the parasite completes invasion (Figure 2j, bottom panel) P113 labelling remains within the parasite. This suggests that P113 is not cleaved from the surface of the parasite during passage through the tight junction and therefore is likely not on the parasite surface, in agreement with Figure 2d and previous studies (Miyazaki et al., 2021).

2.3 | P113 interacts with PTEX and exported cargo

Data presented here indicate that P113 localises to the PV throughout the intraerythrocytic lifecycle. To investigate its function at this location, we therefore completed co-immunoprecipitation (co-IP) assays with P113HA and 3D7 control parasites with a view to identifying specific interacting partners of P113 (Figure 3a). The P113HA line was selected over wild type parasites because the antibody to endogenous P113 recognises the N-terminal domain (Figure 1a) which is likely responsible for protein binding (Campeotto et al., 2020) and therefore the antibody may not be able to bind sufficiently to facilitate detection of interacting proteins. Following co-IP, bound proteins were fractionated by SDS PAGE (Figure 3a) and protein bands that were unique or stronger in the P113HA co-IP were excised and analysed by mass spectrometry (Figure 3a, Tables S3 and S4). Equivalent regions were also excised for the 3D7 co-IP. To analyse the data, proteins found in individual bands of the 3D7 co-IP were removed from the matched bands of the P113 co-IP, unless they were present at >4× (significant

peptides) in the corresponding P113 co-IP bands. Resulting P113 co-IP-specific peptides were then ordered based on protein coverage, and anything lower than 5% protein coverage was discarded. Proteins were then ordered based on the number of significant protein sequences and proteins with non-significant protein sequences were discarded. This left a small number of proteins which were subsequently categorised based on their location within the infected erythrocyte/parasite (Figure 3b, Table S4). From these data, P113 accounted for ~12% of all significant sequences demonstrating that the co-IP worked efficiently. No single protein stood out as being the key interacting partner of P113, however, substantial amounts of PTEX (~12% of total significant protein sequences) and exported proteins destined for the erythrocyte surface (~16% of total significant protein sequences) were detected, as well as numerous parasite surface proteins (MSPs, ~20% of total significant protein sequences) (Figure 3b, Table S4). Since these assays were completed on intracellular parasites (mixed stage culture, predominantly trophozoites and schizonts), the detected MSPs and parasite surface proteins are representative of proteins present at the PPM in intracellular parasites and not the merozoite surface. Collectively, given the distribution of these proteins, these data suggest that P113's function may require interaction with proteins both on the PPM and the PVM faces of the PV space.

Previous studies have demonstrated an interaction between P113 and PTEX (Elsworth et al., 2016), and P113 and an exported, trappable SURFIN 4.1 reporter (Miyazaki et al., 2021). In light of our co-IP data suggesting that P113 spans the PV space and interacts with components of both the PVM and PPM, as well as exported proteins known to traffic through PTEX, we decided to probe the proposed interactions between P113/PTEX and exported proteins. To do this we used a trappable cargo which enables the co-IP of PTEX and its interacting partners during protein export. Specifically, we generated parasites expressing a fusion protein comprising the first 113 amino acids of Hyp1 (PF3D7_0113300) fused to nanoluciferase (Nluc), murine dihydrofolate reductase (mDHFR) and a FLAG epitope tag (Nluc-TRAP, Figure S2c). The Hyp1 leader sequence ensures the protein is exported via PTEX, Nluc serves as a bioluminescent reporter, and murine DHFR is refractory to protein unfolding upon addition of the antifolate compound WR99210 (WR) and thus will cause the cargo to become trapped in PTEX (Charnaud, Jonsdottir, et al., 2018; Gehde et al., 2009; Mesen-Ramirez et al., 2016). WR is normally toxic to wild type parasites, so this construct was transfected into parasites expressing a mutated form of human DHFR that is resistant to WR (Figure S2d). Ring stage parasites expressing the Nluc-TRAP fusion were treated ±10 nM WR for 16 h and whole infected cells were subsequently crosslinked with 2 mM DSP (dithiobis[succinimidyl propionate]). Cells were stringently lysed in 1% SDS (sodium dodecyl sulphate) to solubilise protein complexes, and lysates were diluted to 0.1% SDS prior to FLAG co-IP (Figure 3c). Western blots of eluates probed with a range of antibodies revealed that although

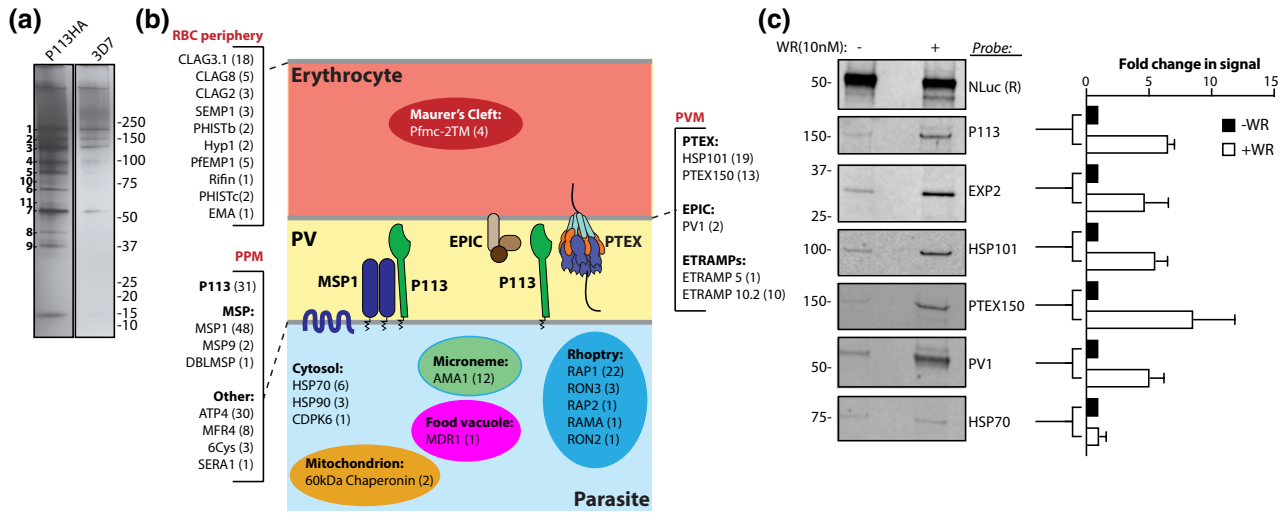

FIGURE 3 P113 interacts with PVM and PPM components, and trapped PTEX cargo. (a) P113HA and 3D7 trophozoite and schizont-stage parasites were used for co-immunoprecipitation assays with anti-HA beads. Bound proteins were eluted and visualised by silver staining. Bands specific to the P113 elution but not 3D7 control were analysed by mass spectrometry (labelled 1–11). (b) Data from (a) were pooled and 3D7 background was removed. Proteins were sorted by protein coverage with a 5% cut-off. Proteins with no significant peptides were removed and the remaining proteins were grouped based on their location within the parasite and are shown in the diagram. Numbers in brackets represent the number of significant peptides detected for that specific protein. (c) P113-*glmS*_Nluc-TRAP parasites were treated ±10 nM WR for 16 h to enable trapping of Nluc-TRAP in PTEX. The FLAG epitope tag of the TRAP construct was subsequently used for co-immunoprecipitation assays. Bound proteins were analysed by western blotting and revealed that PTEX components (EXP2, HSP101 and PTEX150) all co-immunoprecipitated with the trapped cargo, as did EPIC component PV1. P113 is strongly enriched in fractions eluted from cargo trapped in PTEX indicating it associates with PTEX, EPIC and cargo when they are bound for export. Graph represents mean densitometry of bands from three representative co-immunoprecipitation assays with error bars showing ± standard deviation. Values were calculated by setting the densitometry of the WR condition for each individual antibody to 1, and then calculating the fold change upon addition of WR. This was normalised to the fold change seen for Nluc upon addition of WR. R1220 was used to detect P113 (Elsworth et al., 2016)

similar amounts of Nluc-TRAP were co-IP'd via the FLAG tag, core PTEX components EXP2, HSP101 and PTEX150, and the EPIC component PV1 all associated more strongly with the WR-trapped cargo (Figure 3c, +WR). Similar results were observed for P113, whereby its interaction with the Nluc cargo is enhanced when it is trapped in PTEX (Figure 3c, +WR). While these data suggest that P113 interacts with exported cargo either directly or through an interaction with the rest of the PTEX complex, it is also possible that this binding is due to P113 interacting non-specifically with abundant trapped Nluc in its vicinity. Despite this, these data do agree with our mass spectrometry results and implicate a role for P113 in binding export complexes (PTEX and EPIC) and their associated cargo.

2.4 | Knockdown of P113 does not affect protein export

Localisation and co-IP data suggest a role for P113 in protein export. To investigate this further, we generated a parasite line in which we appended a *glmS* riboswitch element (Prommana et al., 2013) to the C-terminus of *p113* (P113-*glmS*) for conditional knockdown of P113 (Figure S2d, Table S1). Addition of glucosamine (GlcN) to the P113-*glmS* parasites activates the *glmS* ribozyme activity resulting in self-cleavage of the messenger RNA (mRNA), loss of the 3′ untranslated region (UTR), and subsequent knockdown of protein expression. We also transfected an exported Nluc (exNluc) into these parasites (Figures 4, S2e) to facilitate quantification of protein export and susceptibility to sorbitol lysis, both of which are associated with PTEX functioning (Beck et al., 2014; Elsworth et al., 2014). The P113-*glmS*_exNluc line and the parental 3D7 parasites containing exNluc (3D7_exNluc), were treated for 72 h from ring stage with increasing concentrations of GlcN to monitor the reduction of P113 (Figure 4a). Western blotting and subsequent densitometric analyses revealed that treatment with 0.5–3 mM GlcN reduced P113 protein levels by ~60–80% in the P113-*glmS*_exNluc line but had no effect on the 3D7_exNluc control strain (Figure 4a). To investigate the effect of P113 knockdown on parasite growth, lactate dehydrogenase (LDH) activity assays were completed over multiple parasite cycles. Resultant data indicated a slight growth delay from cycle 3 onwards (Figure 4b). Specifically, P113-*glmS*_exNLuc parasites noticeably slowed their growth from cycle 3 onwards in a GlcN-titratable manner, and by cycle 4 this difference was statistically significant when compared to the 3D7_exNluc control (3 mM GlcN $p = .0224$, 4 mM GlcN $p = .0012$, as indicated by an Unpaired student's t test).

We next investigated the role of P113 in protein export and new permeability pathway (NPP) activity (sorbitol lysis sensitivity), as both activities rely on PTEX functioning (Beck et al., 2014; Elsworth et al., 2014). To examine exNluc export across the PVM, we utilised the Nluc export assay which quantifiably determines whether a protein is within the erythrocyte cytosol (exported), within the PV space (secreted) or within the parasite (Charnaud, Jonsdottir, et al., 2018; Counihan et al., 2017). P113-*glmS*_exNluc and 3D7_exNluc parasites were treated with GlcN for 48 h (trophozoite to trophozoite) to get a substantial knockdown of P113 protein levels without slowing down the growth of the parasites, to enable direct comparisons between export and sorbitol lysis in the P113-*glmS*_exNluc and the 3D7_exNluc control line (Figure 4c–e). There was no significant difference in Nluc export between the parasite strains at any GlcN concentration tested (Figure 4c). Furthermore, under the same GlcN treatment conditions, export of endogenous skeleton binding protein (SBP1) was not affected and the number of SBP1 puncta detected in the infected erythrocyte was not statistically significantly different across either of the strains for any treatment condition (Figure 4d), indicating there was also no change in the number of Maurer's clefts, key hubs for sorting exported proteins.

No difference was observed in sorbitol sensitivity when P113 was knocked down indicating that the functioning of the NPPs at the

FIGURE 4 Conditional knockdown of P113 reveals no defect in bulk protein export or sorbitol lysis sensitivity. (a) P113-*glmS*_exNluc parasites treated for 72 h with increasing concentrations of GlcN display a conditional depletion of P113 specific to the P113-*glmS*_exNluc strain and not the parental 3D7_exNluc strain. EXP2 was used as a loading control. Far right panel depicts level of P113 protein knockdown as quantified by densitometry completed on P113 and EXP2 specific bands from three independent experiments. Error bars represent ± standard deviation. R1220 was used to detect P113 (Elsworth et al., 2016). (b) LDH assays completed over four cell cycles of GlcN treatment reveal that P113-*glmS*_exNluc but not parental 3D7_exNluc parasites show reduced growth from cell cycle 3. Parasites were treated with GlcN at ring stage and cycle 1 represents trophozoites collected the day following treatment initiation. Data represent three biological replicates completed in technical triplicate. Unpaired Student's t tests were completed and found that the growth in Pf113-*glmS* lines at cycle 4, treated with 3 and 4 mM GlcN was significantly less than the growth of 3D7 at these higher concentrations of GlcN ($p = .0224$ and $p = .0012$ respectively). (c) Export assays completed utilising the exNluc as a marker of protein export demonstrated there was no significant difference in protein export between P113-*glmS*_exNluc and 3D7_exNluc parasites following treatment with GlcN for 48 h. exported Nluc: Nanoluciferase exported into the erythrocyte. Secreted Nluc: Nanoluciferase secreted into the PV. Parasite Nluc: Nanoluciferase retained inside the parasite. Assays were completed in technical duplicate for three biological replicates. (d) P113-*glmS*_exNluc and 3D7_exNluc parasites were treated for 48 h with 0, 1 or 3 mM GlcN and cells were subsequently analysed by IFA with labelling for Maurer's cleft protein SBP1. Specific SBP1 puncta were counted as a marker of native protein export and data indicate there is no significant difference in export of SBP1 in either cell line following treatment with 0, 1 and 3 mM GlcN to knockdown P113. The results are representative of three independent biological experiments where at least 50 cells were counted per condition, per experiment. Scale bars: 2 μm. (e) There was no difference in the lysis of erythrocytes infected with P113-*glmS*_exNluc and exNluc trophozoites following treatment with isotonic 5% sorbitol following the knockdown of P113 with GlcN. This indicates that knockdown of P113 did not reduce the activity of the NPPs in the plasma membrane of infected erythrocytes. Assays were completed in technical triplicate for three biological replicates

infected erythrocyte surface was not affected by P113 knockdown (Figure 4e). Collectively these data demonstrate that P113 knockdown has no effect on protein export via PTEX, and P113 is not an essential component of the protein export machinery.

2.5 | Truncation of P113 has no effect on parasite growth or protein export

Previous research has suggested that P113 needs to be membrane associated and on the merozoite surface to function as a binding partner for Rh5 (Galaway et al., 2017). Here we sought to investigate the importance of the C-terminal putative GPI-anchor domain using the P113HA line (Figure 2a–i). This line contains LoxP sites which flank the C-terminal third of the gene, as well as a DiCre DNA recombinase. Addition of rapamycin dimerises and activates the DiCre recombinase to excise the floxed region, removing the putative GPI anchor (Figure S2a). These parasites were treated with rapamycin to excise the C-terminus of P113, however, the excision rate was so low, we were unable to detect any specific phenotype in the resulting parasite pool. To generate P113 truncation parasites, we therefore treated clonal P113HA ring-stage parasites with 0.4 μM rapamycin for 72 h, and then immediately cloned the treated pool by limiting dilution. Multiple clones in which the C-terminal HA tag had been completely removed were generated (Clones A and B). A clone in which gene excision had

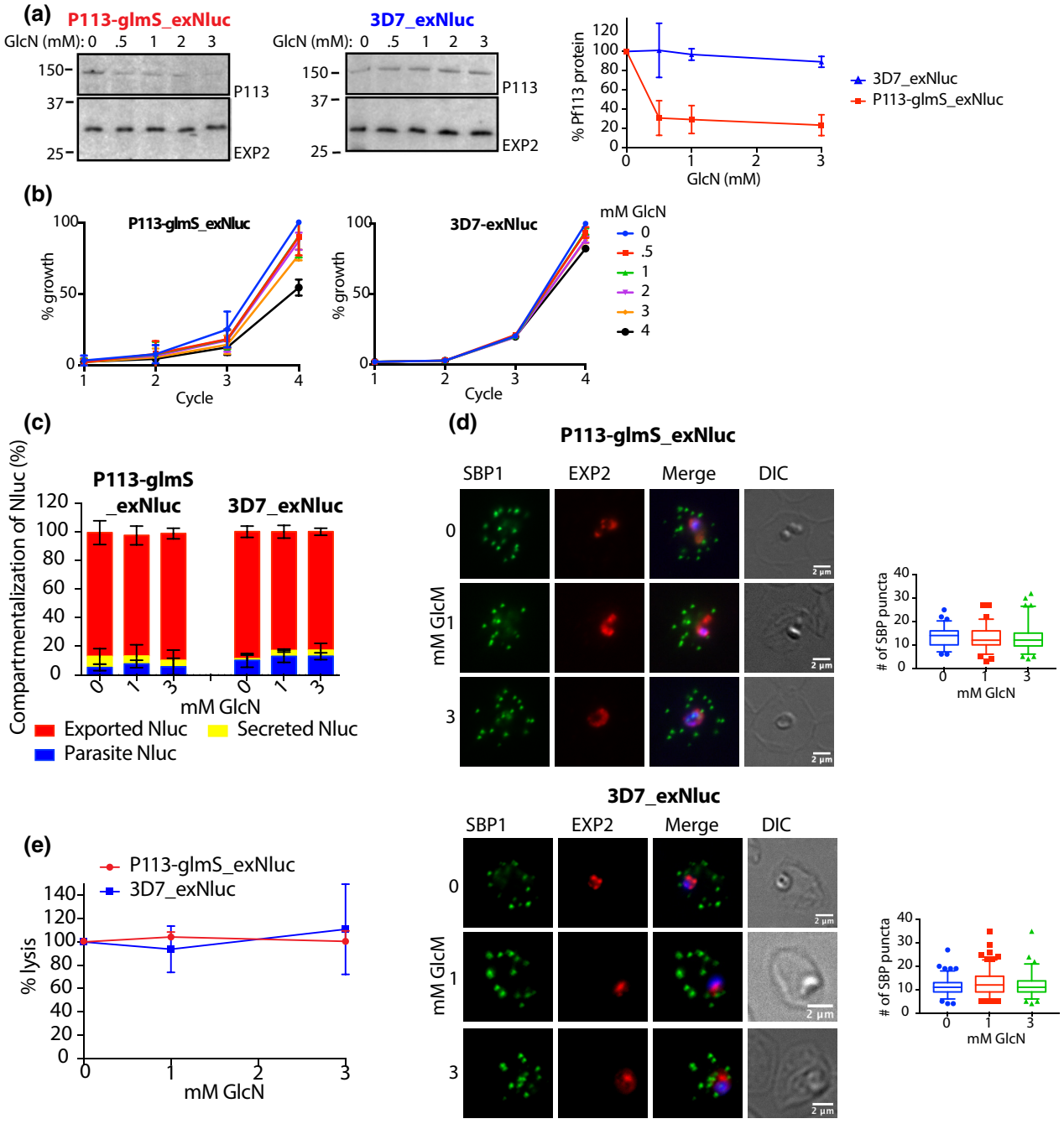

not occurred (Clone C) was used as a control (Figure 5). Western blot analysis revealed that control Clone C retained full length P113HA (Figure 5a), while the excised clones expressed a smaller N-terminal P113 fragment of the expected size following deletion of the C-terminal region detectable by the rabbit P113 antibody (Figure 5a). Clones A and B will be referred to as truncated P113 clones. To confirm that this N-terminal fragment was indeed soluble and therefore possibly non-functional, carbonate extraction assays were performed (Figure 5b). In control clone C and 3D7 parasites, full length P113 partitioned into the carbonate insoluble pellet (Figure 5b) as expected (Figure 1c). A slightly smaller product in Clone C was detected in the soluble fractions, potentially representing a breakdown product of full length P113. The N-terminal truncation product was mostly PBS soluble, although some was also present in the carbonate soluble fraction possibly due to interactions with membrane bound complexes such as PTEX and EPIC (Figure 5b). No P113 was detected in the carbonate pellet for the truncated Clones A and B, indicating these parasites contain mostly soluble, truncated P113 protein which due to a lack of GPI anchoring may no longer be fully functional.

To investigate the overall effect of P113 truncation on parasite growth, the truncated P113 Clones (A, B) and their control (C), as well as a wild type 3D7 parasites, were subjected to multi-cycle growth assays (Figure 5c). LDH assays completed each cycle for a total of five cycles revealed no difference in growth rate between the truncated (Clones A and B) and the control (Clone C) parasites (Figure 5c). Expression of soluble, truncated P113 therefore did not reduce overall parasite growth.

Next, we sought to investigate the effect of truncating P113 on protein export. We were unable to transfect the exNluc construct into the P113 truncation lines as they already contained multiple resistance cassettes, so we instead investigated the export of numerous native proteins exported to the erythrocyte plasma membrane (PfEMP3 and KAHRP) by IFA (Figure 5d). There was no difference in PfEMP3 or KAHRP labelling in P113 truncation parasites compared to their control, we therefore concluded that P113 does not play an essential role in exporting these proteins in vitro.

We also investigated the expression of PfEMP1 on the parasite surface, as this is linked to PTEX activity and therefore possibly P113. To investigate if truncation of P113 had an effect on PfEMP1 trafficking, we measured antibody recognition of surface expressed PfEMP1 by flow cytometry (Chan et al., 2012) using malaria-exposed human samples from Kenyan adults ($n = 24$) (Figure 5e). P113 truncation Clones A and B were analysed alongside their control clone (Clone C), a parental 3D7 parasite line routinely enriched for PfEMP1 expression, and an SBP1 knockout (KO) line, in which PfEMP1 is not surface exposed (Figure 5e). PfEMP1 was still surface expressed in truncated P113 parasites (Figure 5e), and while this was at lower levels than the control 3D7 parasites, it was higher than the negative control SBP1 KO parasites. These data indicate that surface expression of PfEMP1, and therefore its trafficking, still occurs when P113 is truncated.

2.6 | Knockdown or truncation of P113 does not affect parasite invasion of erythrocytes

Previous work completed with recombinant P113 suggested it was involved in parasite invasion by binding to the essential invasion ligand Rh5 (Galaway et al., 2017). To directly investigate the role of native P113 in parasite invasion, we completed invasion assays in both P113-*glmS* and P113 truncation parasites (Figure 6). Specifically, P113 expression was knocked down in the P113-*glmS*_exNluc line by the addition of GlcN for 48 h and following parasite egress, parasites were allowed to invade new erythrocytes over a 4-h window. Infected erythrocytes were then washed to remove free merozoites and incubated for a further 24 h in the absence of GlcN to facilitate parasite growth (Figure 6a). Nanoluciferase activity was measured as an indicator of parasite invasion efficiency and no statistically significant difference in invasion of P113-*glmS*_exNluc parasites compared to control 3D7_exNluc parasites was detected (Figure 6a). Heparin was used as a control and worked as expected, blocking parasite invasion (Figure 6a). These data demonstrate that knockdown of P113 by ~60%–80% had no significant effect on parasite invasion in vitro.

We also completed invasion assays in parasites expressing truncated P113. P113 truncation Clones A and B, control Clone C, and 3D7 control parasites were allowed to invade new erythrocytes over a 4-h window. Erythrocytes were subsequently washed to remove free merozoites and incubated for a further 24 h. Parasitaemia was counted and compared to the parasitaemia prior to invasion to calculate fold change (a measurement of invasion efficiency) for each parasite line. There was no statistically significant difference in the fold change in parasitaemia between any of the lines tested, thus full length P113 does not appear to be essential for parasite invasion in vitro.

2.7 | Disruption of P113 causes morphological disruption of the PVM

Data presented here have shown that P113 is present on the PPM of intracellular parasites, and that it interacts with proteins present on the PVM (PTEX, EPIC, exported proteins), potentially bridging the PV space. Given that P113 does not have an essential role in protein export, we looked more closely at the morphology of parasites expressing truncated or knocked down P113 to glean further insight into the protein's possible function.

Co-labelling IFAs were performed in the P113 truncation mutant (Clone A) and control (Clone C) parasites, as well as a 3D7 wild type control parasites with antibodies specific to P113 (R716) and EXP2 as a marker of the parasite periphery. Resultant images revealed that the N-terminal portion of P113 expressed in the truncated lines remains partially localised to the parasite periphery, as well as throughout the parasite cytosol (Figure 7a). It is therefore possible that the N-terminal domain retains some P113 function. These IFAs were completed on acetone/methanol fixed slides, as this is the optimal condition for R716 labelling. We completed additional IFAs with

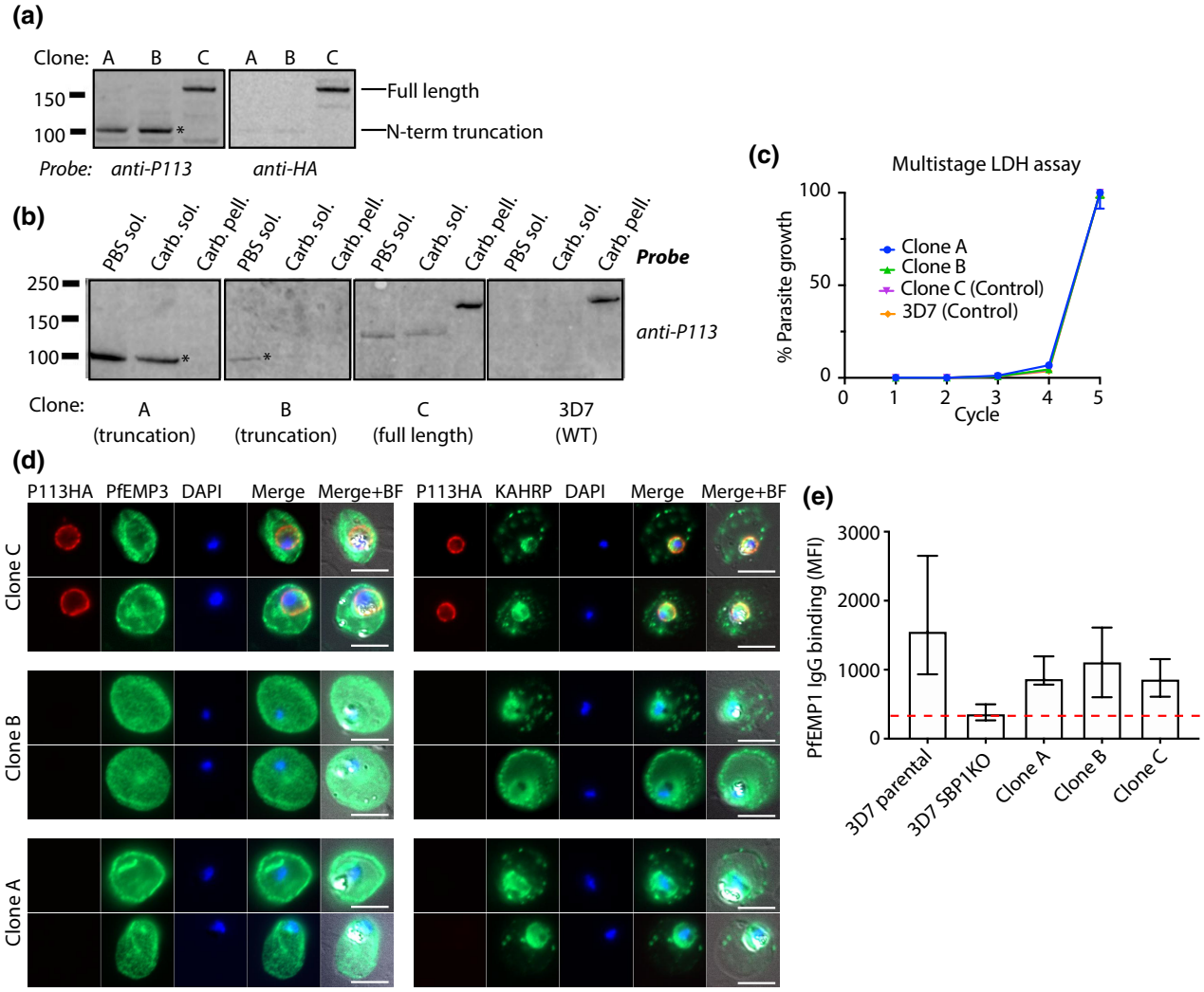

FIGURE 5 Removal of the C-terminal third of P113 does not noticeably reduce parasite growth, and the remaining N-terminal portion is predominantly soluble. (a) Western blot of P113HA Clones A, B and C following rapamycin-induced excision of the C-terminal floxed region of P113HA. DiCre-mediated truncation of the protein has occurred in Clones A and B, while Clone C contains full length P113HA. N-terminal portion of P113 is denoted with *. R1220 was used to detect P113 (Elsworth et al., 2016). (b) Carbonate extraction assays completed on P113 truncation and control lines indicate that the N-terminal fragment remaining post-excision is predominantly soluble, unlike the full length P113 protein which is strongly membrane associated and found in the carbonate pellet. Sol.; soluble. Pell.; pellet. Carb.; carbonate. Controls are shown in Figure 1c. * shows P113 truncation product. R1220 was used to detect P113 (Elsworth et al., 2016). (c) Multi-cycle LDH assays completed over five cell cycles reveal there is no growth defect in the clones expressing truncated P113 when compared to either 3D7 control parasites, or P113HA control parasites (Clone C). Data represent three biological replicates completed in triplicate. (d) Parental control P113HA parasites (Clone C), and P113-truncation lines (Clones A and B) were analysed by IFA for the presence of HA (P113HA C-terminus) and the exported proteins PfEMP3 and KAHRP. There were no obvious differences in exported protein localisation (PfEMP3 and KAHRP). Scale bar: 5 μm. (e) There is no reduction in bulk PfEMP1 export in truncated P113 parasites compared to their parental control. Dashed red line represents background level of PfEMP1 IgG binding in the absence of surface expressed PfEMP1. P113 truncation (Clones A and B) and parental lines (Clone C) all express less PfEMP1 on their surface than the 3D7 control, likely due to having spent a longer time in culture without knob (PfEMP1) selection. IgG levels are expressed as geometric mean fluorescence intensity (MFI). Data represent median and interquartile range ($n = 24$) for two biological replicates completed in technical duplicate

paraformaldehyde/glutaraldehyde fixation as this is optimal for EXP2 labelling. Samples were probed with antibodies specific to the HA tag (full length P113) and the PVM marker EXP2 (Figure 7b). In the control cells, EXP2 labelling (green) appears as a ring of puncta around the parasite corresponding to the PVM (Figure 7b, Clone C). In parasites expressing truncated, soluble P113 (Clones A and B), there were distinct PVM blebs which were statistically significantly more numerous than in the control (Clone A $p < .0001$, Clone B $p < .0001$) (Figure 7b). These data suggest that instead of playing a role in export through its interactions with exported proteins and PTEX/EPIC in the PV space, P113 could instead be using these interactions to stabilise the PVM against the PPM to maintain PVM integrity.

To investigate if the same phenotype was observed when P113 was knocked down, we investigated PVM morphology in the

P113-*glmS*_exNluc parasite line (Figure 7c,d). As a control for GlcN and WR, parasites expressing a HA-tagged copy of HSP101 and an exported Nluc (HSP101HA_Nluc-TRAP) were used. In these parasites, HSP101 is tagged with an HA epitope tag, but not a *glmS* riboswitch and therefore addition of GlcN should not affect protein expression levels. To investigate the PVM morphology in these parasites, P113 expression was conditionally knocked down in the P113*glmS*_exNluc line by addition of GlcN. Parasites in which P113 had been knocked down (+GlcN, bottom two panels) contained significantly more PVM blebs than the untreated (-GlcN, top two panels) parasites (Figure 7c). This effect was due to P113 knockdown rather than the GlcN alone as there was no difference in the number of membrane blebs in the GlcN-treated control HSP101HA_Nluc-TRAP parasites (Figure 7c).

Previous studies have shown that trapping cargo in PTEX at the PVM can lead to the appearance of PVM blebs containing trapped cargo protein (Charnaud, Jonsdottir, et al., 2018). To investigate what happens to these blebs when P113 is knocked down, we conditionally treated parasites with both GlcN to knockdown P113, and WR to trap the exNluc construct in PTEX (Figure 7c, +WR). This treatment further increased the number of PVM-associated blebs detected in the P113*glmS*_Nluc-TRAP line but had no effect on the HSP101HA_Nluc-TRAP control line, indicating that the effect is due to P113 knockdown and not WR or GlcN treatment alone. Analysis of these blebs using super-resolution structured illumination microscopy (SIM) revealed that they contain deposits of both EXP2 and Nluc cargo as has previously been reported for cargo trapped in PTEX (Figure 7d).

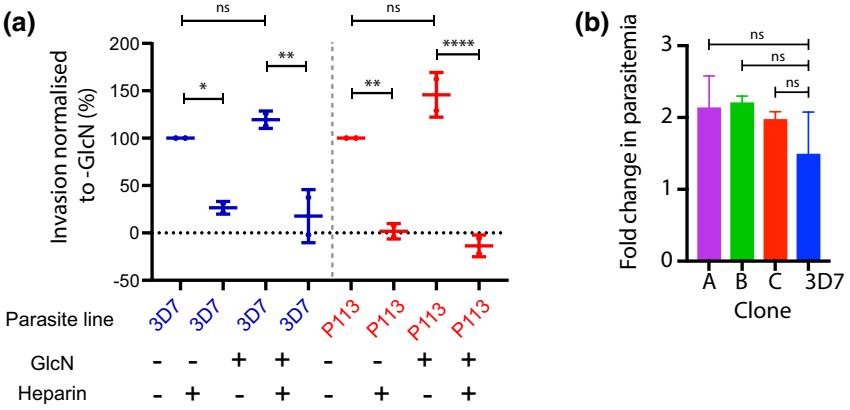

FIGURE 6 P113 is not essential for parasite invasion *in vitro*. (a) P113-*glmS*_exNluc (P113) and 3D7_exNluc (3D7) parasites were treated ±1 mM GlcN for 72 h to knockdown P113 expression and were subsequently used for invasion assays. Nluc activity was used as a marker for successful invasion. Heparin (100 μg/ml) was included as a positive control for invasion inhibition. There was no statistically significant difference in invasion efficiency between ± GlcN in the 3D7 and P113 lines, whereas the addition of heparin to both lines ± GlcN induced a statistically significant reduction in invasion. Error bars represent the standard deviation of two independent biological repeats, each with three technical replicates. The lines untreated with GlcN were normalised to 100%. Statistical analysis was performed via one-way ANOVA. * indicates $p < .05$, ** indicates $p < .01$, **** indicates $p < .0001$. (b) Erythrocyte invasion assays were completed with P113-truncation clones (A, B) where the C-terminal domain has been removed, as well as control lines (Clone C, 3D7). The fold change in parasitaemia following invasion was calculated and there was no significant difference detected between each of the clones as determined by unpaired Student's *t* tests indicating P113 does not play a major role in parasite invasion. Data represent mean from three independent biological replicates. Error bars represent standard deviation

FIGURE 7 Truncation of P113 or conditional knockdown of P113-*glmS* results in production of membranous blebs, exacerbated by the concurrent trapping of cargo. (a) Immunofluorescence analysis of 3D7 wild type, P113HA control (Clone C) and P113 truncation parasites (Clone A) was completed with antibodies labelling P113 (R716) and PVM marker EXP2. Images indicate that some truncated P113 is present at the parasite periphery, and some is present in the parasite cytosol. BF; brightfield. Scale bar: 5um. (b) Parental control P113HA parasites (Clone C), and P113-truncation lines (Clones A, B) were analysed by IFA for the presence of HA (full length P113HA) and EXP2 as a marker of the PVM. In the absence of full length P113 (P113-truncation Clones A and B), EXP2 labelling at the PVM revealed significant morphological abnormalities by way of increased number of PVM blebs in the truncated P113 clones (unpaired Student's *t*-test, ***0.0001). Data based on total cells (A [$n = 74$], B [$n = 114$], C [$n = 131$]) from three biological replicates. Scale bar: 5 μm. (c) P113-*glmS*_Nluc-TRAP and HSP101HA_Nluc-TRAP parasites were treated: -GlcN/-WR, -GlcN/+WR, +GlcN/-WR, or +GlcN/+WR to conditionally knockdown P113 (+GlcN) or TRAP Nluc-TRAP (+WR) in PTEX. Graphs represent the number of membranous blebs extending from the PVM of single cells as indicated by EXP2 labelling, per parasite line, per condition. When P113 was knocked down and the cargo was trapped in PTEX (+GlcN/+WR), the number of blebs significantly increased as calculated using an unpaired Student's *t* test. **$p = .0069$, ***$p = .0002$ ****$p < .0001$, n.s; not significant. Data represent counts from at least 50 cells per parasite line per condition from three biological replicates. Scale bar: 1 μm. (d) SIM images of P113-*glmS*_Nluc-TRAP parasites treated +GlcN/+WR. Membranous blebs are shown to contain both EXP2 (red) and trapped Nluc (green). Scale bar: 1 μm

3 | DISCUSSION

Data presented here reveal that P113 is a PV-resident protein throughout the intraerythrocytic lifecycle, extending from the PPM to the PVM. P113 interacts with PVM-associated export complexes including PTEX and EPIC, as well as a multitude of exported proteins, yet is not essential for protein export in vitro. It also interacts with proteins on the PPM during the intraerythrocytic cycle, however, it is not essential for parasite invasion in vitro as determined by protein knockdown and protein truncation. Instead, P113 appears to play a role in maintaining PVM architecture during the intraerythrocytic lifecycle.

Previous data utilising the AVEXIS (avidity-based extracellular interaction screening) system and recombinantly expressed P113 implicated a role for P113 as a membrane-bound anchor for the essential invasion ligand Rh5 during parasite invasion (Galaway et al., 2017). Here, fluorescence imaging of merozoites did not

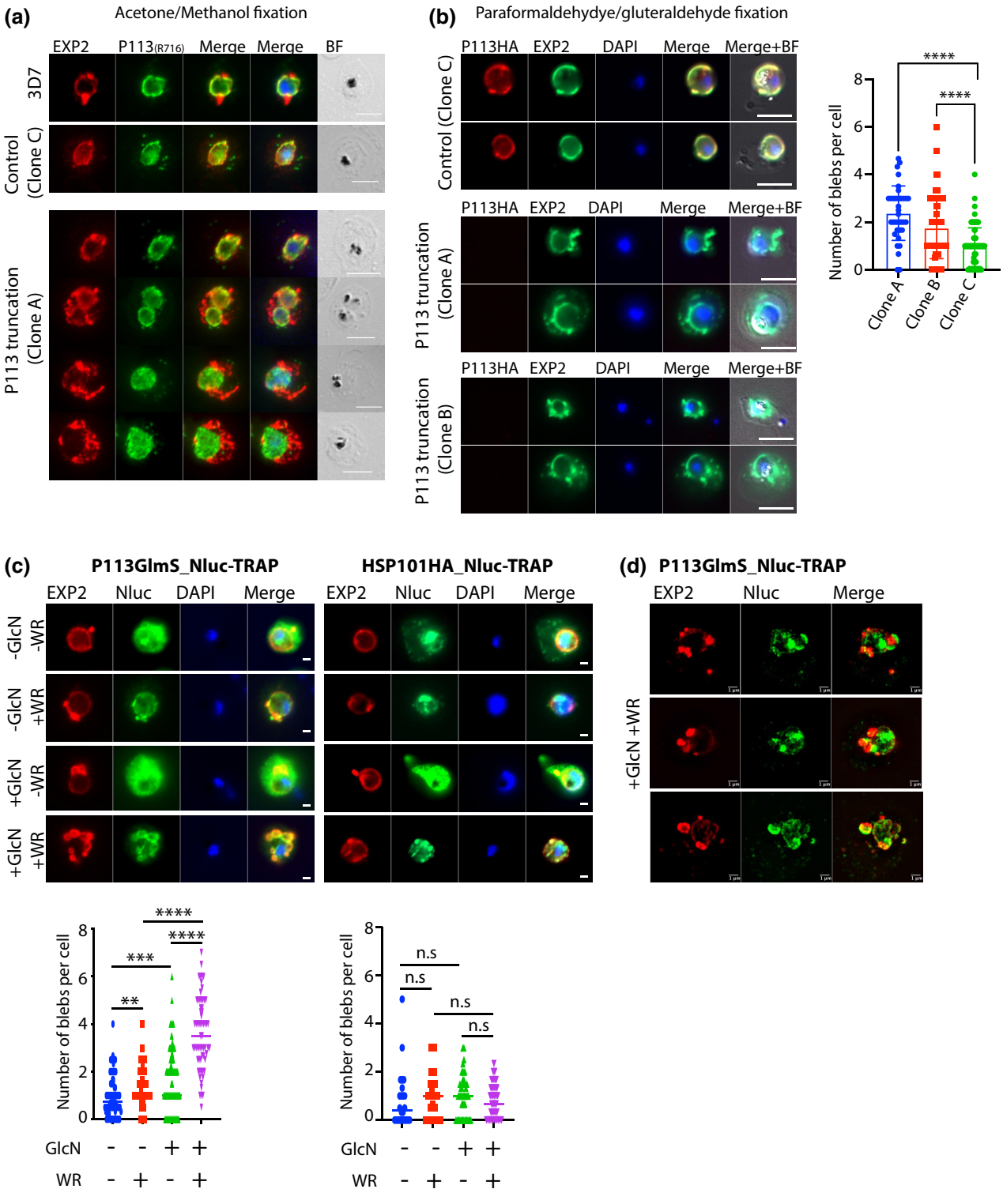

detect an obvious pool of P113 on the merozoite surface, and instead detected P113 most strongly within internal structures both in free merozoites, and in invading merozoites. To determine if P113 might have a role in invasion we generated a parasite strain where the membrane-anchoring portion of the protein was removed (truncated P113), rendering P113 soluble. These parasites had no invasion defect and replicated like wild type parasites. Furthermore, knockdown of P113-*glmS* did not appear to reduce invasion and therefore the data collectively suggest that P113 does not play an important role during invasion *in vitro*. We did not specifically investigate the interaction of P113 with Rh5 in late stage parasites but the fact that in younger parasites P113 appeared to interact with many proteins, does not preclude that P113 might bind to Rh5 during invasion, however, this interaction would likely not be essential for invasion itself.

Co-immunoprecipitation of P113 and subsequent mass-spectrometry based analyses revealed that P113 does not have a single, prominent binding partner and instead co-purifies a wide array of proteins found within the PV space on both the PPM and PVM sides. Here we found P113 to interact with both PTEX and EPIC as has been shown previously (Batinovic et al., 2017; Elsworth et al., 2016), as well as a large pool of exported proteins, which are predominantly destined for export to the erythrocyte surface. From co-IP western blot analyses, P113 appears to interact most strongly with exported cargo during protein export, that is, when the cargo is within PTEX, which is consistent with our proposed role of P113 interacting with components located on the PVM to maintain PVM morphology. It should be noted, however, that due to the abundance of the trapped reporter in the PV space, and the apparent ability of P113 to bind a wide array of proteins, it is possible that these data are reflective of the 'sticky' nature of P113 and are possibly not indicative of a specific PTEX-binding role. Indeed, knockdown of P113 has no effect on protein export, thus any binding between P113 and exported cargo is not likely to be essential for parasite survival. Furthermore, while numerous proteins from the PPM were detected in abundance in our co-IP assays, it is not likely that P113 has specific binding sites for each of these proteins. It is more likely that P113 binds these proteins via its lectin-like N-terminal domain (Campeotto et al., 2020). Interestingly, within these assays we detected substantial amounts of MSPs. This is consistent with our IFA data that show that in mid-schizonts, P113 localises to the PPM which is also where MSPs localise. Rhoptry proteins also represented a substantial proportion of significant peptides detected in our co-IP analyses and again this is concordant with our IFA data, which shows that in late stage schizonts, nascent P113 appears within intracellular puncta which are likely to represent nascent secretory organelles such as rhoptries and dense granules. Rh5 protein sequences were detected, however, they were not significant (four protein sequences, Table S2). Collectively our co-IP data are consistent with P113 being anchored in the PPM and extending across the PV to provide stability to the PVM. Such a role is not unheard of in Apicomplexan parasites. In *T. gondii* the invasion motor protein GAP45 has been found to bridge the PPM and outer leaflet of the inner membrane complex to bind the actin-myosin motor, while maintaining the regular spacing of the two membranes and thus enabling effective actin-myosin motor functioning (Frenal et al., 2010). We propose that P113 plays a similar role to GAP45, but in maintaining the architecture of the PVM.

Truncation of P113 to a form that is no longer membrane associated had a significant effect on PVM morphology, however, this disruption had no effect on parasite growth *in vitro*, nor did it effect bulk export of proteins into the erythrocyte. We detected a similar effect on the PVM when P113 expression was conditionally knocked down (Figure 4). P113 knockdown for four cell cycles moderately reduced parasite growth, suggesting that disruption of the PVM morphology may reduce the fitness of parasites possibly through reducing the efficiency of protein export through PTEX (Beck et al., 2014; Elsworth et al., 2014), or the uptake of nutrients across the PVM (Garten et al., 2018). *In vitro*, perturbation of the rate of protein export would not necessarily be highly detrimental to the parasite, as most exported proteins are involved in immune evasion and therefore not essential for parasite growth *in vitro* (Jonsdottir, Gabriela, et al., 2021; Maier et al., 2008).

Attempts were made to fully disrupt *p113* with a drug selection marker to generate a KO line *in vitro*, however, these attempts were unsuccessful. This does not prove essentiality, however, it does suggest that we may not be able to generate a complete gene KO *in vitro*. This is consistent with mutagenesis studies whereby only the C-terminal portion of P113 could be interrupted, leaving the N-terminus intact (Zhang et al., 2018). IFA analyses presented here indicate that the N-terminal truncated portion of P113 does appear to reside both within the PV and the parasite cytoplasm (Figure 7a) and could therefore maintain some P113 function. Conversely, *p113* has been knocked out *in vivo* in *P. berghei* (Offeddu et al., 2014), the mouse model of malaria. These P113 KO parasites demonstrate reduced sporozoite to liver stage conversion, resulting in reduced merozoite output and a delay to patency (Offeddu et al., 2014). This could be a result of morphological perturbation of the PVM caused by the absence of P113.

The identification of membranous blebs at the PVM associated with P113 perturbation supports previous observations that disruption of normal PV protein expression disrupts PVM morphology (Charnaud, Jonsdottir, et al., 2018; Garten et al., 2018; Mesen-Ramirez et al., 2019). Specific stressors such as trapping protein cargo in PTEX (Charnaud, Jonsdottir, et al., 2018) and conditional knock out of PVM resident protein EXP1(Nessel et al., 2020), can also lead to the production of these structures. The relative contribution of P113 is yet to be determined under each of these conditions, however, our data indicate that trapping cargo in PTEX (+WR) following reduction of P113 (+GlcN) significantly enhanced the formation of these blebs ($p < .0001$) when compared to parasites in which cargo was trapped (+WR) but P113 expression was not altered (-GlcN). Furthermore, in the absence of its membrane anchoring domain, P113 functioning appears to be compromised and the normal PVM morphology where the PVM and PPM are held in close apposition cannot be maintained (Garten et al., 2020). It is possible therefore that the role played by P113 in maintaining PVM architecture is linked to other processes at the PVM, however, further investigations are required to elucidate what precisely these functions may be.

Overall, these data shed light on the role of P113 at the PVM in intracellular parasites and expand the current field of knowledge

relating to the formation of PVM blebs. Further study in this field may ultimately find common links between key players at the PVM and reveal novel mechanisms to be targeted for intervention.

4 | EXPERIMENTAL PROCEDURES

4.1 | Immunofluorescence assays

To capture invading merozoites (Figure 2), samples were prepared as outlined previously (Riglar et al., 2013). For all other IFAs, cells were placed on poly-L-lysine coated coverslips in 24-well plates in filtered PBS and allowed to settle on the coverslip. PBS was subsequently removed and replaced with 4% paraformaldehyde/0.0075% glutaraldehyde in PBS (20 min/room temperature [RT]). Cells were subsequently quenched and permeabilised in 0.1 M glycine pH 7 and 0.02% Triton-X 100 (TX100, Sigma-Aldrich). Following removal of glycine, cells were incubated in blocking buffer (1% casein (Sigma-Aldrich) or 3% bovine serum albumin (BSA, Sigma-Aldrich)), containing 0.02% TX100, in filtered PBS). Primary antibodies (1:500) were subsequently incubated in blocking buffer overnight at 4°C. Following three washes in PBS, AlexaFluor 488 or 594 goat anti-rabbit or mouse secondary antibodies were diluted at 1:3000 in blocking buffer and incubated for 1 h in the dark. Following three further washes with PBS, coverslips were either post-fixed in 4% paraformaldehyde/0.0075% glutaraldehyde in PBS (5 min), quenched with 0.1 M glycine (10 min) and washed twice with PBS before mounting, or mounted directly onto slides with VectaShield (Vector Laboratories) containing 0.1 ng/μl 4′,6–diamidino-2-phenylindole (DAPI, Invitrogen). Images were taken with either a Zeiss Axio Observer Z1 inverted widefield microscope, or a Nikon Structured Illumination Microscope and processed and analysed with Fiji software. For analysis of merozoites, Z-Stacks were deconvolved and cropped (3 × 3 μm) in ImageJ, maximum Z-projections were generated through the cell for each cropped Z-stack and separate (not deconvolved) reference differential interference contrast (DIC) images were aligned, cropped and merged with maximum Z-projections to produce merged fluorescence/DIC images. Pearson's correlation coefficients were used to measure colocalisation of two antibodies using ImageJ software. An r value of 1 represents complete colocalisation and an r value of 0 represents no colocalisation. Analysis was done on raw images and the same exposure settings were maintained for each experiment. Antibodies listed in Table S2.

4.2 | Protease protection assays

Protease protection assays were completed as outlined in (Sanders et al., 2019) and the same *Homo sapiens* HSP70 (HsHSP70) and EXP2 mAb controls were used. Briefly, magnet purified trophozoites (24–30 h post-infection [hpi]) were pelleted prior to resuspension in un-supplemented RPMI-HEPES. Pellet was split into 12 equal fractions and re-pelleted prior to removal of RPMI-HEPES. Four tubes were subsequently treated with recombinant EQT, four tubes were treated with EQT and 0.03% saponin; and the remaining four tubes were treated with EQT and 0.25% TX100. Following incubation at RT for 10 min, PK was added to various final concentrations; 0, 1, 5 and 20 μg/ml and incubated for 15 min at 37°C. Reaction was stopped by addition of 200 μl of Complete Protease Inhibitor Cocktail (PI, Roche) containing 1 mM PMSF. Following centrifugation, pellet material was separated from supernatant which was subsequently concentrated using Centricon concentrator columns. Samples were analysed by western blotting. Antibodies listed in Table S2.

4.3 | Multi-cycle lactate dehydrogenase activity (LDH) assays

Lactate dehydrogenase activity was measured to determine parasite biomass as described previously (Makler et al., 1993). Briefly, ring-stage parasites were synchronised and adjusted to 2% haematocrit and 0.3% parasitaemia with increasing concentrations of GlcN (0–3 mM). The next day when the parasites were trophozoites, samples of each GlcN treatment were taken (cycle one) and stored at −80°C. The remainder of the cells were allowed to continue growing and samples removed every 48 h for four cycles. Following standard LDH assay (Makler et al., 1993), absorbance was measured with a plate reader at 560 nm (Thermo Scientific Fisher Inc.). Data presented represents three (*glmS* assays) or five (LoxP assays) biological replicates completed in technical triplicate.

4.4 | Export assays

Performed and calculated as in (Counihan et al., 2017). Briefly, synchronous P113-*glmS*_exNluc or 3D7_exNluc parasites expressing exported Nluc (Azevedo et al., 2014) were treated with 0–3 mM GlcN at trophozoite stage (~24–36 hpi) for 48 h. Infected erythrocytes were subsequently transferred to a 96-well plate with GlcN levels maintained and cells at 1% haematocrit, 1% parasitaemia. Background luminescence and possible quenching of Nluc signal in the various buffers was controlled for by addition of a series of wells containing only wild type parasite-infected erythrocytes spiked with recombinant Nluc (1 ng/μl). Standard export assays were completed as previously described (Counihan et al., 2017). Two technical replicates were completed for each of three biological replicates and data were analysed as outlined in (Counihan et al., 2017).

4.5 | Sorbitol lysis assays

Performed and analysed as in (Counihan et al., 2017). Briefly, P113-*glmS*_exNluc or 3D7_exNluc parasites expressing exported Nluc (Azevedo et al., 2014) were treated with 0–3 mM GlcN at trophozoite stage (~24–36 hpi) for 48 h. After washing the parasites in 2×PBS, 10 μl at 1% haematocrit was dispensed in triplicate into a Greiner Lumitrac 96-well microplate and loaded into a Clariostar luminometer (BMG

labtech). To each well, either 40 µl PBS (control) or 40 µl of sorbitol lysis buffer containing NanoGlo substrate (280 mM sorbitol, 20 mM Na-HEPES, 0.1 mg/ml BSA, pH 7.4, Nano-Glo™ [1:1000 dilution]) was added and the relative light units (RLU) measured every 3 min with gain set to 2500. Data were analysed using Prism GraphPad software. Data shown represent three biological replicates completed in technical triplicate.

4.6 | Cargo-trapping in P113-*glmS*_Nluc-TRAP

P113-*glmS*_Nluc-TRAP and HSP101HA_Nluc-TRAP parasites were sorbitol synchronised and the following day at trophozoites, were treated with either 0 mM or 1 mM GlcN. The following day when parasites were rings, they were further treated ± 10 nM WR keeping the GlcN concentrations constant. Parasites were allowed to grow for another 16 h to facilitate the trapping of Nluc-TRAP in WR-treated samples and were subsequently fixed and prepared for IFAs as outlined above. Primary antibodies included rabbit anti-Nluc (1:1000) and mouse anti-EXP2 (1:1000) as listed in Table S2.

4.7 | Cargo-trapping immunoprecipitation assays

P113-*glmS*_Nluc-TRAP parasites were grown to ring stage and synchronised by standard sorbitol synchronisation. Parasites were split into two equal fractions and treated ± 10 nM WR overnight (16–20 h treatment to facilitate cargo trapping). Parasites were subsequently crosslinked and whole infected cells were used as input for the immunoprecipitation (to ensure equal Nluc-TRAP input per condition). To crosslink parasites, infected erythrocytes pellets (~1 ml) were resuspended in 10 ml PBS containing 2 mM DSP (Sigma-Aldrich) and crosslinking performed as described previously (Bullen et al., 2012). Crosslinked pellets were subsequently resuspended in 1 ml 1% SDS at RT for 1 h. Insoluble material was removed by pelleting, lysate was transferred to 10 ml tubes and diluted to 0.1% SDS by addition of 9 ml PBS with PI. Anti-FLAG M2 affinity gel (Merck) was washed three times in 0.5% TX100 in PBS prior to addition to lysate overnight at 4°C. Following binding, FLAG gel was pelleted and unbound material removed. Gel was washed three times in 0.5% TX100 in MicroBioSpin columns (BioRad) and bound proteins were eluted in 80 µl NRSB. Prior to western blotting, crosslinker was reduced by boiling the samples in 200 µM DTT at 80°C for 4 h prior to loading 40 µl per sample on 4–12% bis-tris gels as described above. Resultant blots were probed as outlined in individual panels. Antibodies listed in Table S2.

4.8 | P113HA immunoprecipitation assays

Mixed stage P113HA and 3D7 parasites were harvested by saponin lysis, resuspended in 20× pellet volume lysis buffer (0.5% TX100 in PBS with PI) and incubated at RT for 1 h. Insoluble material was pelleted, and sample collected as input. Anti-HA agarose (Sigma Aldrich) was added to lysate and incubated overnight at 4°C. Following binding, agarose was pelleted (1000 g for 1 min) and unbound material was removed. Agarose was washed 4× in 1 ml 0.5% TX100 in PBS with PI to remove remaining unbound fraction. Bound proteins were eluted by addition of 2× NRSB and subsequently electrophoresed as described above. Eluted proteins were visualised with the Pierce silver stain kit, mass spectrometry grade (Thermo Fisher) as per manufacturer's instructions. Bands specific to P113HALoxP were excised and gel slices were reduced with 10 mM tris(2-carboxyethyl) phosphine (TCEP) in 50 mM triethylammonium bicarbonate (TEAB) at 55°C for 45 min and then washed 3×1 ml 50 mM TEAB for 15 min. Samples were subsequently alkylated with 55 mM iodoacetamide (IAM) in 50 mM TEAB for 30 min at RT then washed 3×1 ml for 15 min in 25 mM TEAB prior to the addition of 80 µl of mass spectrometry grade Trypsin (Pierce) at 4 µg/µl overnight at 37°C. Digested peptides were acidified to a final concentration of 1% trifluoroacetic acid and bound to C18 resin, washed and eluted. Eluents were concentrated down to 20 µl in a speed vacuum centrifuge. Peptide concentration was determined by BCA protein assay (Thermo Fisher) and adjusted to a final concentration of 0.5 µg/µl with 0.1% trifluoroacetic acid prior to analysis by LC–MS/MS as described previously (Jonsdottir, Counihan, et al., 2021).

4.9 | Invasion assays

To induce knockdown of P113, 1 mM GlcN was added to P113-*glmS*_exNluc line and control line 3D7_exNluc (Azevedo et al., 2014) at trophozoite stage, which was conducted in parallel with their matched untreated controls. The invasion assay was performed as per (Dans et al., 2020) whereby 48 h after GlcN treatment, schizonts were purified using a 60% Percoll (Cytiva) density gradient and added back to uninfected erythrocytes with GlcN to a final parasitaemia and haematocrit of 1–2% and 1% respectively. Prior to the incubation for invasion, samples of whole culture were taken to measure Nluc signal to account for any differences between lines in the assay set-up which was used in the calculation of invasion rate (see below). Plates were incubated at 37°C for 4 h to allow merozoite egress and invasion to occur. Cells were then treated with sorbitol, and three washes in media were performed before incubating the culture at 37°C for a further 24 h without GlcN until parasites were > 24 h hpi. To determine invasion rate, whole cells (5 µl) at 1% haematocrit were dispensed into white 96-well luminometer plates and 45 µl of 1× NanoGlo Lysis Buffer containing 1:1000 NanoGlo substrate (Promega) was injected into wells. RLU was measured by a CLARIOstar luminometer (BMG Labtech). Analysis was performed by subtracting the background control (Dans et al., 2020), before values were normalised to the starting parasitaemia for each line ± GlcN. Invasion of the GlcN treated lines was then expressed as a percentage of their untreated matched controls. Heparin was added during the 4 h invasion window at 100 µg/ml as a positive control for invasion inhibition.

For P113-truncation clones (Clone A and B) and control lines (3D7 and Clone C), invasion assays were performed following Percoll

purification as described above. The invasion rate was then measured by blinded manual counts of newly invaded ring stage parasites from Giemsa-stained blood smears after a 4 h invasion window.

ACKNOWLEDGEMENTS

This work was supported by the Victorian Operational Infrastructure Support Program received by the Burnet Institute. We acknowledge the Australian Red Cross Blood Bank for the provision of human blood. M.G.D is a recipient of an Australian Government Research Training Program Scholarship, T.K.J. is a recipient of a Melbourne Research Scholarship, M.G. is a recipient of a Deakin University Postgraduate Research Scholarship, and T.F.dK-W is an NHMRC Senior Research Fellowship. We thank Jude Przyborski for the PV1 antibody, Brian Cooke for the SBP1 antibody and Monash Micro Imaging (MMI) for assistance with microscopy. We are grateful to Steven Batinovic, Matthew Dixon and Leann Tilley for providing PV1-HA *P. falciparum* parasites. We thank Rasika Kumarasingha for technical assistance. We acknowledge the generous assistance provided by the Mass Spectrometry and Proteomics Facility at The University of Melbourne, Bio21 Institute. This work was funded by National Health and Medical Research Council Project Grant APP1128198. Open access publishing facilitated by The University of Melbourne, as part of the Wiley - The University of Melbourne agreement via the Council of Australian University Librarians.

ETHICS STATEMENT

Ethics approval was obtained from the Alfred Hospital Human Research and Ethics Committee, Australia, Institutional Review Board for Human Investigation at University Hospitals of Cleveland for Case Western Reserve University, USA and the Ethical Review Committee at the Kenya Medical Research Institute. Written informed consent was obtained from all study participants or their parents or legal guardians.

DATA AVAILABILITY STATEMENT

The data that supports the findings of this study are available in the supplementary material of this article.

ORCID

Hayley E. Bullen https://orcid.org/0000-0003-4923-3019
Jake Baum https://orcid.org/0000-0002-0275-352X

REFERENCES

Azevedo, M.F., Nie, C.Q., Elsworth, B., Charnaud, S.C., Sanders, P.R., Crabb, B.S. et al. (2014) Plasmodium falciparum transfected with ultra bright NanoLuc luciferase offers high sensitivity detection for the screening of growth and cellular trafficking inhibitors. *PLoS One*, *9*, e112571.

Batinovic, S., McHugh, E., Chisholm, S.A., Matthews, K., Liu, B., Dumont, L. et al. (2017) An exported protein-interacting complex involved in the trafficking of virulence determinants in plasmodium-infected erythrocytes. *Nature Communications*, *8*(16), 044.

Beck, J.R., Muralidharan, V., Oksman, A. & Goldberg, D.E. (2014) PTEX component HSP101 mediates export of diverse malaria effectors into host erythrocytes. *Nature*, *511*, 592–595.

Bullen, H.E., Charnaud, S.C., Kalanon, M., Riglar, D.T., Dekiwadia, C., Kangwanrangsan, N. et al. (2012) Biosynthesis, localization, and macromolecular arrangement of the plasmodium falciparum translocon of exported proteins (PTEX). *Journal of Biological Chemistry*, *287*, 7871–7884.

Campeotto, I., Galaway, F., Mehmood, S., Barfod, L.K., Quinkert, D., Kotraiah, V. et al. (2020) The structure of the cysteine-rich domain of plasmodium falciparum P113 identifies the location of the RH5 binding site. *mBio*, *11*(5), e01566-20.

Chan, J.A., Howell, K.B., Reiling, L., Ataide, R., Mackintosh, C.L., Fowkes, F.J. et al. (2012) Targets of antibodies against plasmodium falciparum-infected erythrocytes in malaria immunity. *Journal of Clinical Investigation*, *122*, 3227–3238.

Charnaud, S.C., Jonsdottir, T.K., Sanders, P.R., Bullen, H.E., Dickerman, B.K., Kouskousis, B. et al. (2018) Spatial organization of protein export in malaria parasite blood stages. *Traffic*, *19*, 605–623.

Charnaud, S.C., Kumarasingha, R., Bullen, H.E., Crabb, B.S. & Gilson, P.R. (2018) Knockdown of the translocon protein EXP2 in plasmodium falciparum reduces growth and protein export. *PLoS One*, *13*, e0204785.

Chisholm, S.A., McHugh, E., Lundie, R., Dixon, M.W., Ghosh, S., O'Keefe, M. et al. (2016) Contrasting inducible knockdown of the auxiliary PTEX component PTEX88 in P. falciparum and P. berghei unmasks a role in parasite virulence. *PLoS One*, *11*, e0149296.

Combet, C., Blanchet, C., Geourjon, C. & Deleage, G. (2000) NPS@: network protein sequence analysis. *Trends in Biochemical Sciences*, *25*, 147–150.

Counihan, N.A., Chisholm, S.A., Bullen, H.E., Srivastava, A., Sanders, P.R., Jonsdottir, T.K. et al. (2017) *Plasmodium falciparum* parasites deploy RhopH2 into the host erythrocyte to obtain nutrients, grow and replicate. *eLife*, *6*, e23217.

Counihan, N.A., Modak, J.K. & de Koning-Ward, T.F. (2021) How malaria parasites acquire nutrients from their host. *Frontiers in Cell and Developmental Biology*, *9*(649), 184.

Dans, M.G., Weiss, G.E., Wilson, D.W., Sleebs, B.E., Crabb, B.S., de Koning-Ward, T.F. et al. (2020) Screening the medicines for malaria venture pathogen box for invasion and egress inhibitors of the blood stage of plasmodium falciparum reveals several inhibitory compounds. *International Journal for Parasitology*, *50*, 235–252.

Elsworth, B., Matthews, K., Nie, C.Q., Kalanon, M., Charnaud, S.C., Sanders, P.R. et al. (2014) PTEX is an essential nexus for protein export in malaria parasites. *Nature*, *511*, 587–591.

Elsworth, B., Sanders, P.R., Nebl, T., Batinovic, S., Kalanon, M., Nie, C.Q. et al. (2016) Proteomic analysis reveals novel proteins associated with the plasmodium protein exporter PTEX and a loss of complex stability upon truncation of the core PTEX component, PTEX150. *Cellular Microbiology*, *18*, 1551–1569.

Frenal, K., Polonais, V., Marq, J.B., Stratmann, R., Limenitakis, J. & Soldati-Favre, D. (2010) Functional dissection of the apicomplexan glideosome molecular architecture. *Cell Host and Microbe*, *8*, 15.

Galaway, F., Drought, L.G., Fala, M., Cross, N., Kemp, A.C., Rayner, J.C. et al. (2017) P113 is a merozoite surface protein that binds the N terminus of *Plasmodium falciparum* RH5. *Nature Communications*, *8*(14), 333.

Garten, M., Beck, J.R., Roth, R., Tenkova-Heuser, T., Heuser, J., Istvan, E.S. et al. (2020) Contacting domains segregate a lipid transporter from a solute transporter in the malarial host–parasite interface. *Nature Communication*, *11*, 3825.

Garten, M., Nasamu, A.S., Niles, J.C., Zimmerberg, J., Goldberg, D.E. & Beck, J.R. (2018) EXP2 is a nutrient-permeable channel in the vacuolar membrane of plasmodium and is essential for protein export via PTEX. *Nature Microbiology*, *3*, 1090–1098.

Gehde, N., Hinrichs, C., Montilla, I., Charpian, S., Lingelbach, K. & Przyborski, J.M. (2009) Protein unfolding is an essential requirement for transport across the parasitophorous vacuolar membrane of plasmodium falciparum. *Molecular Microbiology*, *71*, 613–628.

Hakamada, K., Nakamura, M., Midorikawa, R., Shinohara, K., Noguchi, K., Nagaoka, H. et al. (2020) PV1 protein from plasmodium falciparum exhibits chaperone-like functions and cooperates with Hsp100s. *International Journal of Molecular Sciences*, *21*, 8616.

Hakamada, K., Watanabe, H., Kawano, R., Noguchi, K. & Yohda, M. (2017) Expression and characterization of the plasmodium translocon of the exported proteins component EXP2. *Biochemical and Biophysical Research Communications*, *482*, 700–705.

Ho, C.M., Beck, J.R., Lai, M., Cui, Y., Goldberg, D.E., Egea, P.F. et al. (2018) Malaria parasite translocon structure and mechanism of effector export. *Nature*, *561*, 70–75.

Jonsdottir, T.K., Counihan, N.A., Modak, J.K., Kouskousis, B., Sanders, P.R., Gabriela, M. et al. (2021) Characterisation of complexes formed by parasite proteins exported into the host cell compartment of plasmodium falciparum infected red blood cells. *Cell Microbiol*, *23*, e13332.

Jonsdottir, T.K., Gabriela, M., Crabb, B.S., de Koning-Ward, T.F. & Gilson, P.R. (2021) Defining the essential Exportome of the malaria parasite. *Trends in Parasitology*, *37*, 664–675.

de Koning-Ward, T.F., Dixon, M.W., Tilley, L. & Gilson, P.R. (2016) Plasmodium species: master renovators of their host cells. *Nature Reviews Microbiology*, *14*, 494–507.

de Koning-Ward, T.F., Gilson, P.R., Boddey, J.A., Rug, M., Smith, B.J., Papenfuss, A.T. et al. (2009) A newly discovered protein export machine in malaria parasites. *Nature*, *459*, 945–949.

Maier, A.G., Rug, M., O'Neill, M.T., Brown, M., Chakravorty, S., Szestak, T. et al. (2008) Exported proteins required for virulence and rigidity of plasmodium falciparum-infected human erythrocytes. *Cell*, *134*, 48–61.

Makler, M.T., Ries, J.M., Williams, J.A., Bancroft, J.E., Piper, R.C., Gibbins, B.L. et al. (1993) Parasite lactate dehydrogenase as an assay for plasmodium falciparum drug sensitivity. *American Journal of Tropical Medicine and Hygiene*, *48*, 739–741.

Matthews, K., Kalanon, M., Chisholm, S.A., Sturm, A., Goodman, C.D., Dixon, M.W. et al. (2013) The plasmodium translocon of exported proteins (PTEX) component thioredoxin-2 is important for maintaining normal blood-stage growth. *Molecular Microbiology*, *89*, 1167–1186.

Matthews, K.M., Kalanon, M. & de Koning-Ward, T.F. (2019) Uncoupling the threading and unfoldase actions of plasmodium HSP101 reveals differences in export between soluble and insoluble proteins. *mBio*, *10*, e01106-19.

Matz, J.M., Matuschewski, K. & Kooij, T.W. (2013) Two putative protein export regulators promote plasmodium blood stage development in vivo. *Molecular and Biochemical Parasitology*, *191*, 44–52.

Mesen-Ramirez, P., Bergmann, B., Tran, T.T., Garten, M., Stacker, J., Naranjo-Prado, I. et al. (2019) EXP1 is critical for nutrient uptake across the parasitophorous vacuole membrane of malaria parasites. *PLoS Biology*, *17*, e3000473.

Mesen-Ramirez, P., Reinsch, F., Blancke Soares, A., Bergmann, B., Ullrich, A.K., Tenzer, S. et al. (2016) Stable translocation intermediates jam global protein export in plasmodium falciparum parasites and link the PTEX component EXP2 with translocation activity. *PLoS Pathogens*, *12*, e1005618.

Miyazaki, S., Chitama, B.A., Kagaya, W., Lucky, A.B., Zhu, X., Yahata, K. et al. (2021) *Plasmodium falciparum* SURFIN4.1 forms an intermediate complex with PTEX components and Pf113 during export to the red blood cell. *Parasitology International*, *83*, 102358.

Morita, M., Nagaoka, H., Ntege, E.H., Kanoi, B.N., Ito, D., Nakata, T. et al. (2018) PV1, a novel plasmodium falciparum merozoite dense granule protein, interacts with exported protein in infected erythrocytes. *Scientific Reports*, *8*, 3696.

Nessel, T., Beck, J.M., Rayatpisheh, S., Jami-Alahmadi, Y., Wohlschlegel, J.A., Goldberg, D.E. et al. (2020) EXP1 is required for organisation of EXP2 in the intraerythrocytic malaria parasite vacuole. *Cell Microbiology*, *22*, e13168.

Offeddu, V., Rauch, M., Silvie, O. & Matuschewski, K. (2014) The plasmodium protein P113 supports efficient sporozoite to liver stage conversion in vivo. *Molecular and Biochemical Parasitology*, *193*, 101–109.

Prommana, P., Uthaipibull, C., Wongsombat, C., Kamchonwongpaisan, S., Yuthavong, Y., Knuepfer, E. et al. (2013) Inducible knockdown of plasmodium gene expression using the glmS ribozyme. *PLoS One*, *8*, e73783.

Richard, D., MacRaild, C.A., Riglar, D.T., Chan, J.A., Foley, M., Baum, J. et al. (2010) Interaction between *Plasmodium falciparum* apical membrane antigen 1 and the rhoptry neck protein complex defines a key step in the erythrocyte invasion process of malaria parasites. *Journal of Biological Chemistry*, *285*(14), 815–822.

Riglar, D.T., Rogers, K.L., Hanssen, E., Turnbull, L., Bullen, H.E., Charnaud, S.C. et al. (2013) Spatial association with PTEX complexes defines regions for effector export into plasmodium falciparum-infected erythrocytes. *Nature Communication*, *4*, 1415.

Sanders, P.R., Cantin, G.T., Greenbaum, D.C., Gilson, P.R., Nebl, T., Moritz, R.L. et al. (2007) Identification of protein complexes in detergent-resistant membranes of plasmodium falciparum schizonts. *Molecular and Biochemical Parasitology*, *154*, 148–157.

Sanders, P.R., Dickerman, B.K., Charnaud, S.C., Ramsland, P.A., Crabb, B.S. & Gilson, P.R. (2019) The N-terminus of EXP2 forms the membrane-associated pore of the protein exporting translocon PTEX in plasmodium falciparum. *Journal of Biochemistry*, *165*, 239–248.

Sanders, P.R., Gilson, P.R., Cantin, G.T., Greenbaum, D.C., Nebl, T., Carucci, D.J. et al. (2005) Distinct protein classes including novel merozoite surface antigens in raft-like membranes of plasmodium falciparum. *Journal of Biological Chemistry*, *280*(40), 169–176.

Volz, J.C., Yap, A., Sisquella, X., Thompson, J.K., Lim, N.T., Whitehead, L.W. et al. (2016) Essential role of the PfRh5/PfRipr/CyRPA complex during plasmodium falciparum invasion of erythrocytes. *Cell Host & Microbe*, *20*, 60–71.

Weiss, G.E., Gilson, P.R., Taechalertpaisarn, T., Tham, W.H., de Jong, N.W., Harvey, K.L. et al. (2015) Revealing the sequence and resulting cellular morphology of receptor-ligand interactions during plasmodium falciparum invasion of erythrocytes. *PLoS Pathogens*, *11*, e1004670.

WHO. (2021) World Malaria Report.

Wong, W., Huang, R., Menant, S., Hong, C., Sandow, J.J., Birkinshaw, R.W. et al. (2019) Structure of *Plasmodium falciparum* Rh5-CyRPA-Ripr invasion complex. *Nature*, *565*, 118–121.

Yam, X.Y., Birago, C., Fratini, F., Di Girolamo, F., Raggi, C., Sargiacomo, M. et al. (2013) Proteomic analysis of detergent-resistant membrane microdomains in trophozoite blood stage of the human malaria parasite *Plasmodium falciparum*. *Mol Cell Proteomics*, *12*, 3948–3961.

Zhang, M., Wang, C., Otto, T.D., Oberstaller, J., Liao, X., Adapa, S.R. et al. (2018) Uncovering the essential genes of the human malaria parasite plasmodium falciparum by saturation mutagenesis. *Science*, *360*, eaap7847.

SUPPORTING INFORMATION

Additional supporting information may be found in the online version of the article at the publisher's website.

How to cite this article: Bullen, H. E., Sanders, P. R., Dans, M. G., Jonsdottir, T. K., Riglar, D. T., Looker, O., Palmer, C. S., Kouskousis, B., Charnaud, S. C., Triglia, T., Gabriela, M., Parkyn Schneider, M., Chan, J-A, de Koning-Ward, T. F., Baum, J., Kazura, J. W., Beeson, J. G., Cowman, A. F., Gilson, P. R. & Crabb, B. S. (2022). The *Plasmodium falciparum* parasitophorous vacuole protein P113 interacts with the parasite protein export machinery and maintains normal vacuole architecture. *Molecular Microbiology*, *117*, 1245–1262. https://doi.org/10.1111/mmi.14904